

ALMA MATER STUDIORUM - UNIVERSITY OF BOLOGNA

SCHOOL OF ENGINEERING AND ARCHITECTURE

Second Cycle Degree in
Telecommunications Engineering

Master Thesis in
Satellite Communication And Navigation Systems

NB-IoT Synchronization Procedure Analysis

Author:

Riccardo Campana

Supervisor:

Prof. Ing. **Alessandro Vanelli Coralli**

Co-supervisor:

Dr. **Matteo Conti**

Co-supervisor:

Dr. **Carla Amatetti**

Academic Year 2019/2020

Graduation Session III

To my beloved parents and sister

Contents

Introduction	1
1 Narrowband IoT	3
1.1 Deployments Options	4
1.1.1 Stand-Alone Mode of Operation	4
1.1.2 In-Band Mode of Operation	4
1.1.3 Guard-Band Mode of Operation	5
1.2 Physical Layer	5
1.2.1 Frequency Framing	5
1.2.2 Time Framing	6
1.2.3 Downlink Structure	6
1.2.4 Uplink Structure	9
1.3 Protocol Overview	10
1.4 Energy Saving Procedures	11
1.4.1 DRX and eDRX	12
1.4.2 Power Saving Mode (PSM)	14
1.5 Downlink Synchronization	14
1.5.1 NPSS: Time and Frequency Synchronization	15
1.5.2 NSSS: PCID and Initial Frame Synchronization	16
1.6 Random Access Procedure	17
1.6.1 Random Access Preamble	18
1.7 Uplink/Downlink Transmission Procedure	22
1.7.1 Uplink Transmission Procedure	22
1.7.2 Downlink Transmission Procedure	23
2 Satellite NB-IoT Service Provision	25
2.1 System Architecture	26

2.1.1	Transparent Payload	26
2.1.2	Regenerative Payload	27
2.2	Orbits	28
2.2.1	Geostationary Orbit	28
2.2.2	Low Earth Orbit	29
2.2.3	GEO and LEO Scenarios Comparison	30
2.3	Reference Scenario	31
2.4	Doppler	31
2.4.1	Differential Doppler	32
2.4.2	Differential Doppler Assessment	34
2.5	Doppler Mitigation Techniques	35
2.5.1	Frequency Advance	36
2.5.2	CP Based and Map Based Estimation	37
2.5.3	Position Tracking	38
2.5.4	Resource Allocation Strategy	38
2.6	Round Trip Time	39
2.7	Differential Propagation Delay	40
2.8	Delay Implications on NB-IoT Procedures	42
2.8.1	Large RTT Implications on RA Procedures	42
2.8.2	Large RTT Implications on HARQ Procedures	43
2.8.3	DPD Implications on TA Procedure	43
2.8.4	DPD Implications on RA Procedures	44
2.9	DPD Mitigation Techniques	45
2.9.1	Position Tracking	46
2.9.2	New NPRACH Configurations	46
3	Downlink Synchronization Implementation	47
3.1	NPSS Detection Algorithm	47
3.2	NSSS Detection Algorithm	52
3.3	Complexity Evaluation	54
3.3.1	Complexity Of Time Delay Estimation	54
3.3.2	Complexity Of CFO Estimation	54
3.3.3	Complexity Of PCID detection	55
3.3.4	Required UE computational power	55
3.4	Performances	56
3.4.1	Time Delay Probability Of Error	57

<i>CONTENTS</i>	iii
3.4.2 PCID Detection Probability Of Error	59
4 Conclusions	63
Bibliography	65

Nomenclature

AWGN	Additive White Gaussian Noise
BS	Base Station
CFO	Carrier Frequency Offset
CN	Core Network
DCI	Downlink Control Information
DFT	Discrete Fourier Transform
DPD	Differential Propagation Delay
DRX	Discontinuous Reception
eDRX	extended Discontinuous Reception
eNB	Evolved Node B, the LTE base station (BS)
eNodeB	Evolved Node B
FFT	Fast Fourier Transform
FPO	Floating Point Operations
GEO	Geostationary Earth Orbit
GNSS	Global Navigation Satellite System
GW	Gateway
HAPS	High-Altitude Platform Station
HARQ	Hybrid Automatic Repeat Request

LEO	Low Earth Orbit
LoS	Line of Sight
LPWAN	Low Power Wide Area Networks
MAC	Medium Access Control
MIB	Master Information Block
MIB-NB	Master Information Block
ML	Maximum Likelihood
NDI	New Data Indicator
NPBCH	Narrowband Physical Broadcast Channel
NPDCCH	Narrowband Physical Downlink Control Channel
NPDSCH	Narrowband Physical Downlink Shared Channel
NPRACH	Narrowband Physical Random Access Channel
NPSS	Narrowband Primary Synchronization Signal
NPUSCH	Narrowband Physical Uplink Shared Channel
NSSS	Narrowband Secondary Synchronization Signal
NTN	Non Terrestrial Networks
OAI	Open Air Interface
OFDMA	Orthogonal Frequency-Division Multiple-Access
PAPR	Peak To Average Power Ratio
PCID	Physical Cell Identity
PF	Paging Frames
PH	Paging Hyperframes
PHY	Physical
PO	Paging Occasions

PRBs	Physical Resource Blocks
PSM	Power Saving Mode
PTW	Paging Time Window
RA	Random Access
RAP	RA Preamble
RAR	RA Response
RF	Radio Frequency
RFN	Radio Frame Number
RRC	Radio Resource Control
RTT	Round Trip Time
RU	Resource Unit
Sat	Satellite
SatCom	Satellite Communications
SC-FDMA	Single-Carrier Frequency-Division Multiple-Access
SFN	System Frame Number
SIB-NB	System Information Block
SNR	Signal to Noise Ratio
TA	Timing Advance
TB	Transport Block
TBS	Transport Block Size
ToA	Time of Arrival
UE	User Equipment
ZC	Zadoff-Chu

List of Figures

1.1	In-band and guard-band deployment options.	5
1.2	Time framing [1].	7
1.3	Single-carrier time framing [1].	7
1.4	Downlink resource grid, [2].	8
1.5	Downlink frame.	9
1.6	Uplink resource grid, [3].	10
1.7	Uplink frame, [4].	10
1.8	Overview of NB-IoT protocol procedures.	12
1.9	DRX and eDRX current profile, [5].	13
1.10	PSM current profile, [5].	13
1.11	Downlink Synchronization procedure.	15
1.12	NPSS and NSSS frame time occurrence, [1].	16
1.13	NPSS detection method.	17
1.14	NSSS detection method.	18
1.15	Connection Procedure.	19
1.16	Coverage classes, [6].	20
1.17	Symbol group and frequency hopping pattern, [1].	20
1.18	preamble detection method.	21
1.19	Uplink Transmission Procedure.	23
1.20	Downlink Transmission Procedure.	23
1.21	Example of uplink transmission scheduling.	24
1.22	Example of downlink transmission scheduling.	24
2.1	NB-IoT NTN with transparent payload, [7].	27
2.2	NB-IoT NTN with regenerative payload, [7].	28
2.3	Geosynchronous and geostationary orbits.	29
2.4	LEO at different inclinations.	29

2.5	LEO satellite footprint typology, [7].	30
2.6	Doppler curves of reference UEs, $h_{SAT} = 600km$, [8].	35
2.7	Doppler curves of reference UEs, $h_{SAT} = 1500km$, [8].	35
2.8	Doppler shift analysis, [8].	36
2.9	Residual differential Doppler, [9].	37
2.10	System geometry for DPD computation, [7].	42
2.11	Timing Advance analysis, [8].	44
2.12	Cell radius vs Cell center elevation angle, [7].	45
3.1	h and t extraction in one OFDM symbol.	50
3.2	Representation of the considered N_f frames.	53
3.3	NPSS detection simulator scheme without accumulation.	58
3.4	NPSS detection simulator scheme with accumulation of four frames.	58
3.5	NPSS detection simulator scheme without accumulation.	59
3.6	Simulation results for P_e^{delay} without accumulation.	61
3.7	Simulation results for P_e^{delay} with accumulation of four frames.	61
3.8	Comparison between P_e^{delay} with accumulation and without accumulation.	62
3.9	Simulation results for $P_e^{PCID} _{Sync}$ on a window of four frames.	62

List of Tables

1.1	NPRACH formats characteristics.	19
2.1	Nomenclature for Doppler analyzes.	33
2.2	Simulation Parameters.	34
2.3	Maximum values for τ_k , [9].	37
2.4	Reference LEO scenario: $h_{sat} = 600km$, [8].	40
2.5	Reference LEO scenario: $h_{sat} = 1500km$, [8].	40
2.6	GEO scenario: $h_{sat} = 35786km$, [8].	41
2.7	One-way propagation delay and RTT for the considered scenarios, [8].	41
3.1	Values considered for computational power assessment.	56

Introduction

The Internet of Things (IoT) is part of a digital transformation which affects our entire society, including industries as well as consumers and the public sector. Since it provides the capability to interact with the physical world by means of remote sensing and actuation, it provides better insights on the monitored environment and immediate actuation. Therefore, the IoT is an enabler in the revolution of the management of physical processes, making them more efficient. According to the forecasts of [10], 29 billion connected devices are expected by 2022 of which around 18 billion will be related to IoT. Connected IoT devices include machines, health wearable, meters (water, electric, gas, or parking), connected cars, sensors, point-of-sales terminals, consumer electronics, and so on.

IoT applications may be divided into short-range and wide-area depending on the size of their deployment area. In the former the devices are deployed in a limited area and are connected to the network through the means of unlicensed radio technologies, such as ZigBee, Wi-Fi, and Bluetooth. In the latter, for which the deployment area is theoretically unlimited, the connection to the network mostly relies on cellular networks.

The Third Generation Partnership Project (3GPP), recognizing the importance of IoT, introduced a number of key features to supporting it since Release 13. In particular, since 2017 the so called NB-IoT has been launched, providing progressively improved support for Low Power Wide Area Networks (LPWAN).

While terrestrial technologies will play a key role in the provision of the NB-IoT service, satellite networks can have a complementary role thanks to their very wide coverage area and short service deployment time. Within the aforementioned framework, the aim of this thesis is to analyze the feasibility of integrating the NB-IoT technology with satellite communication (SatCom) systems, focusing in particular in the assessment of the downlink synchronization procedure in the NB-IoT SatCom systems. For this reason, this work investigates the issues introduced by the integra-

tion between the NB-IoT terrestrial network and Non Terrestrial Networks (NTN). Furthermore, in order to find possible solutions to harmonize their coexistence, the state of the art of the satellite channel effect mitigation techniques is analyzed. After that, the implementation of a MATLAB simulator for the cell synchronization procedure is presented, as a first step for the understanding of the whole NB-IoT procedures.

The thesis is divided in four chapters. In the first one, a description of the NB-IoT technology will be provided, thus, the protocol procedures and the Physical layer operation will be analyzed. In the second chapter, the main characteristics of SatCom systems will be presented. Afterwards, the main satellite channel characteristics and the implication on the NB-IoT protocol will be investigated. In the third chapter, the NB-IoT synchronization procedures and the implementation of the simulator will be analyzed, then, the simulation results will be presented. The last chapter contains the conclusions and future works.

Chapter 1

Narrowband IoT

LTE technology is designed for high data rates and low latency, implying high complexity for user equipment and higher-power consumption. These characteristics are not suitable for IoT applications, which are characterized by low data rates and sporadic transmission of small data payloads. Indeed, NB-IoT is designed as a simplified version of the full-fledged LTE system. This allows to keep the protocol as simple as possible, in order to meet the goals of long device battery lifetime, extended coverage, and low hardware cost. Although NB-IoT is based on existing LTE functionalities, it is a new technology thus not completely backward compatible with the existing 3GPP standard. Despite this, NB-IoT can be deployed in the same eNodeB (eNB) used for LTE, providing pervasive coverage.

The cost of User Equipment (UE) modem is mainly related to the complexity of the Radio Frequency (RF) and baseband sections. For what concerns NB-IoT baseband processing, it has been kept simple by considering a small Transport Block¹ (TB) size and by relaxing the processing time requirements compared to LTE. Regarding RF, all performance goal of NB-IoT can be achieved with single TX-RX antenna, a low accuracy oscillator and an on-chip low-power amplifier [11].

Long device battery lifetime comes along with low power consumption. IoT applications require infrequent transmission of short packets, thus the time in which the UE has no data to transmit or receive, called idle period, is longer than the active time. Since energy consumption during idle mode is much lower with compared to active periods, increasing the time between active periods, allows to significantly reduce energy consumption. In this regard, some techniques increasing the idle

¹In LTE and NB-IoT the Transport Block is the payload which is passed between the MAC layer and Physical Layer [1].

periods duration are adopted in NB-IoT, as described in Section 1.3.

Improved indoor and outdoor coverage has been achieved by trading off data rate for coverage. In fact, repetitions are used to ensure higher system reliability even in challenging locations for coverage, however, this implies a lower data rate. Furthermore, NB-IoT uses a close to constant envelope waveform in the uplink, thus reducing the waste of power due to amplifier inefficiencies [12][1].

1.1 Deployments Options

As previously mentioned, NB-IoT must have the capability of working in parallel with a legacy LTE service as well as being compatible for the deployment in GSM spectrum. Thus, three different deployments options has been designed for NB-IoT: stand-alone, guard-band and in-band.

1.1.1 Stand-Alone Mode of Operation

NB-IoT is in stand-alone mode of operation when it is deployed as a stand-alone carrier, using any available spectrum with bandwidth of at least 180 kHz. This is exceptionally useful for GSM operators who can deploy NB-IoT in a GSM carrier, refarming part of their spectrum. In this type of deployment, NB-IoT has to be compliant with the GSM spectral mask thus its bandwidth becomes 200 KHz. Furthermore, a guard band of 100 KHz is recommended between GSM and NB-IoT bands, bringing the total refarmed bandwidth to 400 KHz corresponding to two GSM carriers.

1.1.2 In-Band Mode of Operation

In in-band mode of operation NB-IoT is deployed in the existing LTE networks, using one of the LTE Physical Resource Blocks (PRBs). The PRB is the smallest schedulable unit in most downlink cases and it consists of 12 subcarriers for a total bandwidth of 180 KHz. NB-IoT uses the same modulation and numerology as LTE so it is possible to set a NB-IoT 180 KHz carrier in a LTE PRB without degrading the system performances (without account for PRB number reduction). An example of in-band operation mode is shown in Figure 1.1b.

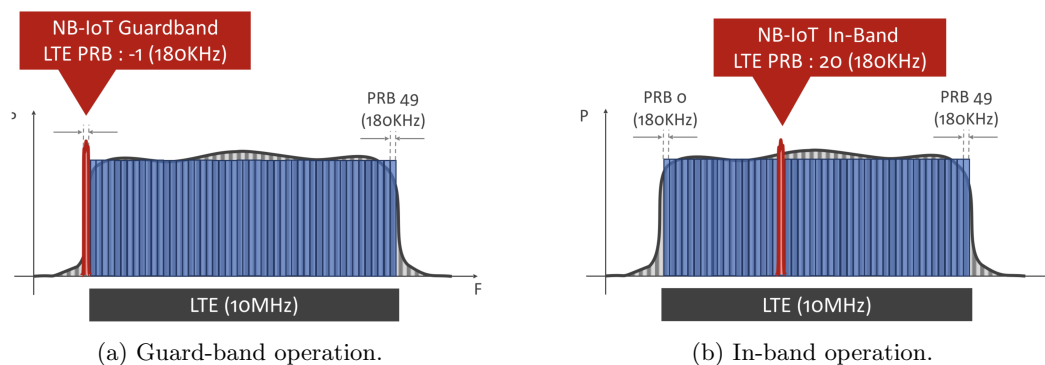


Figure 1.1: In-band and guard-band deployment options.

1.1.3 Guard-Band Mode of Operation

In guard-band mode of operation NB-IoT is deployed in the guard-band of the existing LTE networks. It relies on the fact that LTE deployment occupies only 90% of its total bandwidth, leaving a 5% available at each side. It is therefore possible to place a NB-IoT carrier in the guard band of LTE, as shown in Figure 1.1a.

1.2 Physical Layer

1.2.1 Frequency Framing

A NB-IoT carrier has a bandwidth of 180 KHz, independently from the deployment mode used. A carrier carrying essential physical signals that allow a device to perform cell selection is referred to as an anchor carrier. Although only the anchor carrier is strictly required, multicarrier operation is supported. The additional carriers are named non-anchor carrier and does not carry the physical channels that are required for UE initial cell selection.

In case of in-band or guard-band deployment, the placement of an NB-IoT anchor carrier in frequency is based on a 100 KHz channel raster², just as for LTE. Contrary to LTE, due to the particular bandwidth of a NB-IoT carrier, an NB-IoT anchor carrier can, however, be located slightly off the 100 kHz channel raster. This fixed positions of carriers in frequency is important since, at start-up, a UE needs to search for anchor carriers in order to select an eNB to camp on. Thus, the UE

²In a system that employs a 100 KHz channel raster the carrier center frequency must be an integer multiple of 100 kHz.

can rely on the frequency raster to search for anchor carrier easier.

Furthermore, NB-IoT supports a subcarrier spacing of 15 KHz and 3.75 KHz, implying a carrier subdivision in 12 or 48 subcarriers respectively.

1.2.2 Time Framing

As for the 15 KHz subcarrier spacing, the time unit for the NB-IoT frame is the slot, which is 0.5 ms long. Two slots constitute a subframe and ten subframes constitute a frame, which is 10 ms long (Figure 1.2). While, for the 3.75 KHz subcarrier spacing, the time unit is the slot, which is 2ms long, and five slots constitute a frame of 10 ms, as in Figure 1.3.

Furthermore, 1024 frames constitute a hyperframe and 1024 hyperframes constitute a hyperframe cycle which is the highest level of time frame structure [12].

1.2.3 Downlink Structure

As for the downlink, NB-IoT supports only the subcarrier spacing of 15 KHz, which means that in a band of 180 KHz 12 subcarriers can be allocated. In this case the PRB consists of 12 subcarriers in frequency and one subframe in time, as shown in Figure 1.4, [13][12].

Orthogonal Frequency-Division Multiple-Access (OFDMA) is employed in downlink. In order to ensure backward compatibility NB-IoT is designed with the same LTE numerologies. For instance, the same subcarrier spacing, slot, subframe, and frame duration are employed, as well as for OFDM symbol and cyclic prefix duration. The main difference dwells in the modulation and in coding scheme adopted; in fact, QPSK modulation and convolutional coding with 1/3 coding rate are employed, [14].

The messages exchanged on the physical layer between UE and eNB are divided in channels, and each physical channel is in charge of deliver a specific message typology. Furthermore, they are time-multiplexed in a frame, and each channel is scheduled and allocated to an entire subframe and it uses all the 12 subcarriers. A typical structure is depicted in Figure 1.5.

Downlink physical channels are described in the following:

- *NPBCH*: Narrowband Physical Broadcast Channel is used to deliver the NB-IoT Master Information Block (MIB), which provides essential information for

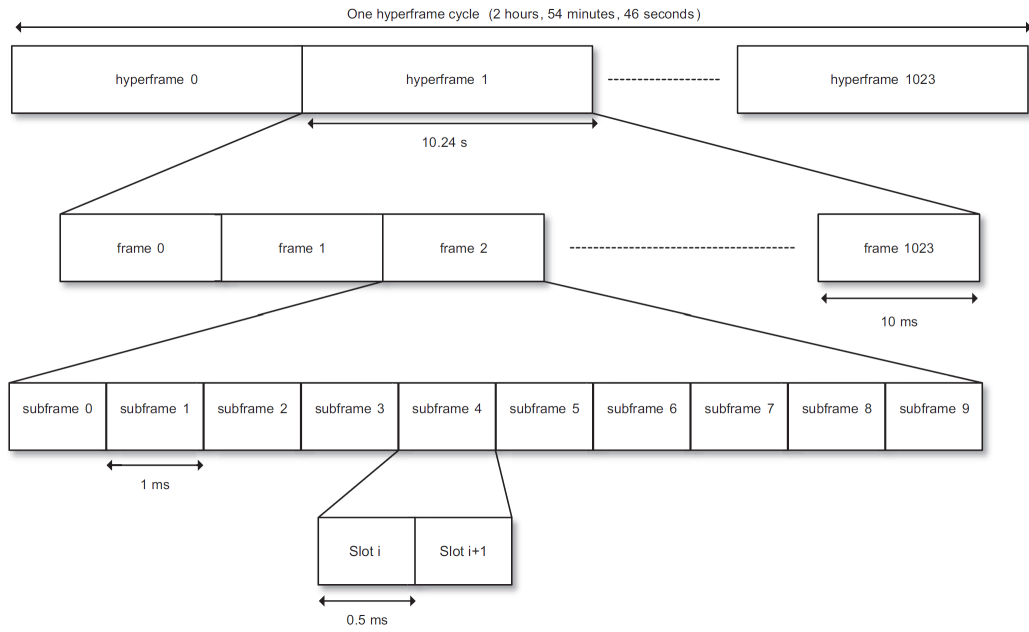


Figure 1.2: Time framing [1].

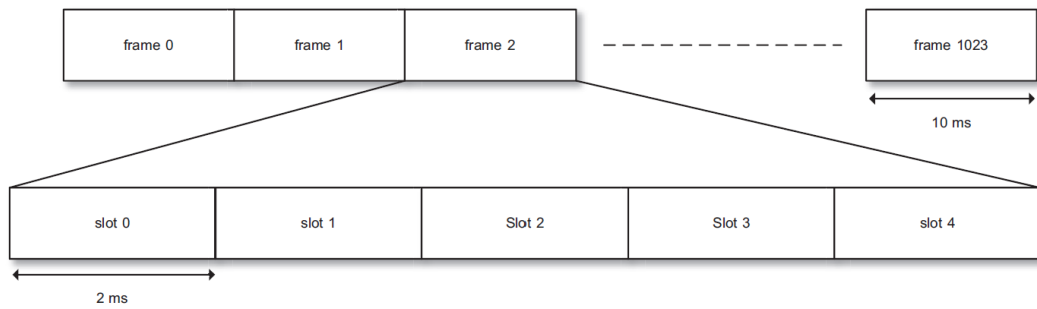


Figure 1.3: Single-carrier time framing [1].

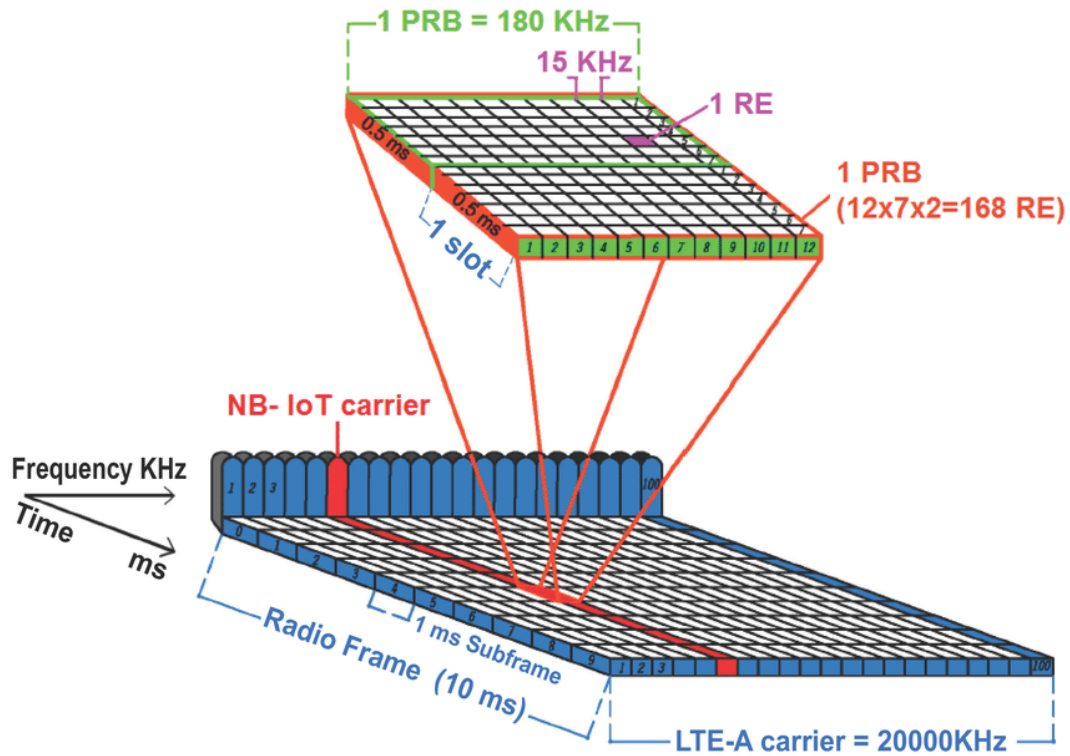


Figure 1.4: Downlink resource grid, [2].

the device to operate in the NB-IoT network.

- *NPDCCH*: Narrowband Physical Downlink Control Channel is used to carry downlink control information. In detail, it delivers uplink grant information, downlink scheduling information and paging information.
- *NPDSCH*: Narrowband Physical Downlink Shared Channel is used to transmit unicast data.
- *NPSS*: Narrowband Primary Synchronization Signal is used by the device to achieve synchronization, in both time and frequency, to an NB-IoT cell.
- *NSSS*: Narrowband Secondary Synchronization Signal is used to detect the Physical Cell Identity (PCID) and acquire more information about the frame structure.

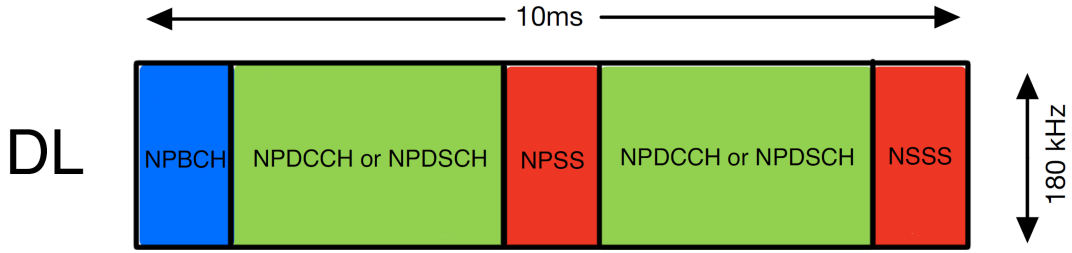


Figure 1.5: Downlink frame.

1.2.4 Uplink Structure

As for the uplink, NB-IoT can operate in multi-tone or in single-tone mode. For multi-tone mode, a 15 KHz subcarrier spacing is used while, for single-tone mode, is used a 3.75 KHz subcarrier spacing. Furthermore, sub-PRB transmission is introduced in uplink, so the smallest uplink schedulable unit is named Resource Unit (RU) and can have different dimensions. In the basic case, where 12 subcarriers using a spacing of 15 kHz are allocated, the RU corresponds to the downlink PRB seen in Figure 1.4. In the case of sub-PRB scheduling assignments of 6, 3, or 1 subcarrier, the RU is expanded in time to compensate for the diminishing frequency allocation. In single-tone allocation, the subcarrier spacing can be 15 KHz or 3.75 KHz, in the latter the RU spans 32 ms in time. Figure 1.6 shows all the different types of uplink RU, with their bandwidth and corresponding time duration, [12][1].

The uplink is based on Single Carrier Frequency Division Multiple Access (SC-FDMA), also known as Discrete Fourier Transform (DFT) Spread OFDM (DFTS-OFDM). Considering the 15 KHz subcarrier spacing the numerology remains the same as in downlink. For what concerns the modulations, $\pi/4$ -QPSK or $\pi/2$ -BPSK are used in conjunction a 1/3 turbo coding. These types of modulation have a very low Peak to Average Power Ratio (PAPR) allowing the transmission with low power backoff. In the extended coverage domain, in which every transmitted watt is important, the power amplifier efficiency introduced by a low PAPR is crucial, [15].

An example of uplink slot format is shown in Figure 1.7. It can be seen that, in case of sub-PRB scheduling, more than one RU can be scheduled in a single time interval.

Uplink physical channels are described in the following:

- *NPUSCH*: Narrowband Physical Uplink Shared Channel is used to carry uplink user data or control information from higher layers.

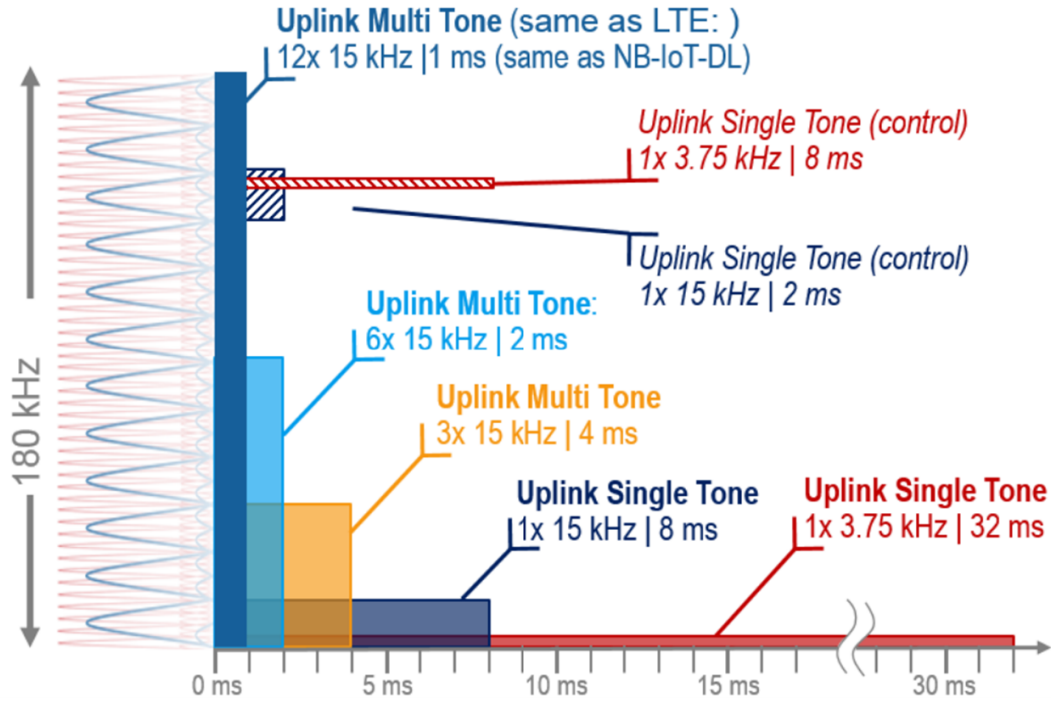


Figure 1.6: Uplink resource grid, [3].

- *NPRACH*: Narrowband Physical Random Access Channel is used by the device to initiate connection and allows the serving base station to estimate the Time of Arrival (ToA) of the received NPRACH signal.

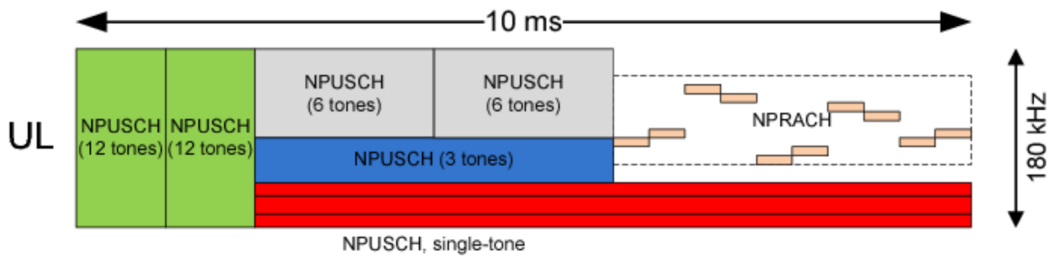


Figure 1.7: Uplink frame, [4].

1.3 Protocol Overview

An overview of NB-IoT protocol procedures, divided in four macro areas, is shown in Figure 1.8. The first two are called Idle mode procedure while the last two are the connected mode procedures.

- *Downlink synchronization*: at start-up the UE performs cell selection, searching and selecting a cell to camp on. Then, it synchronises with the chosen eNB using his broadcast signals: NPSS, NSSS, Master Information Block (MIB-NB) and System Information Block (SIB-NB).
- *Paging monitoring*: the Paging Message (PM) is a message sent through NPDCCH if the eNB needs to connect with the UE. For example in case of data exchange or for system information updating. Thus, UE periodically listens for possible paging messages from eNB on . The periodicity depends on the eDRX or PSM specific configuration.
- *Connection*: UE goes in connected mode if it receives the Paging message or if has UL data to transmit. During connection, the UE asks for radio resources and receives other physical layer settings. In this phase we have the random access procedure, when the UE contends the radio resources with the other UEs that need them.
- *Data exchange*: the eNB sends scheduling information to UE. That radio resources are then used to transmit and receive data and acknowledgements.

1.4 Energy Saving Procedures

NB-IoT user equipment hardware is designed to have a low power consumption in the active state³. However, protracting the active state over time could lead to a quick battery drain. For this reason, 3GPP introduced in NB-IoT some power saving techniques which can extend the battery lifetime.

The user equipment has three main states: active, idle and sleep. In active state the UE absorbs the maximum amount of power due to its transmission and reception activity. In Idle state the UE is on, but the RF section is switched sleep and all the activities are reduced to the minimum. Thus the idle state is characterized by a much lower power consumption. Finally, in the sleep state only a wake up counter is active, thus the power consumption is close to zero.

Therefore, alternating active, idle, and sleep states it is possible to reduce the average power consumption of the UEs. The duty cycle of these different phases is related to the service to deliver. In fact, the longer one is the idle time compared

³In the active state the UE is transmitting or receiving.

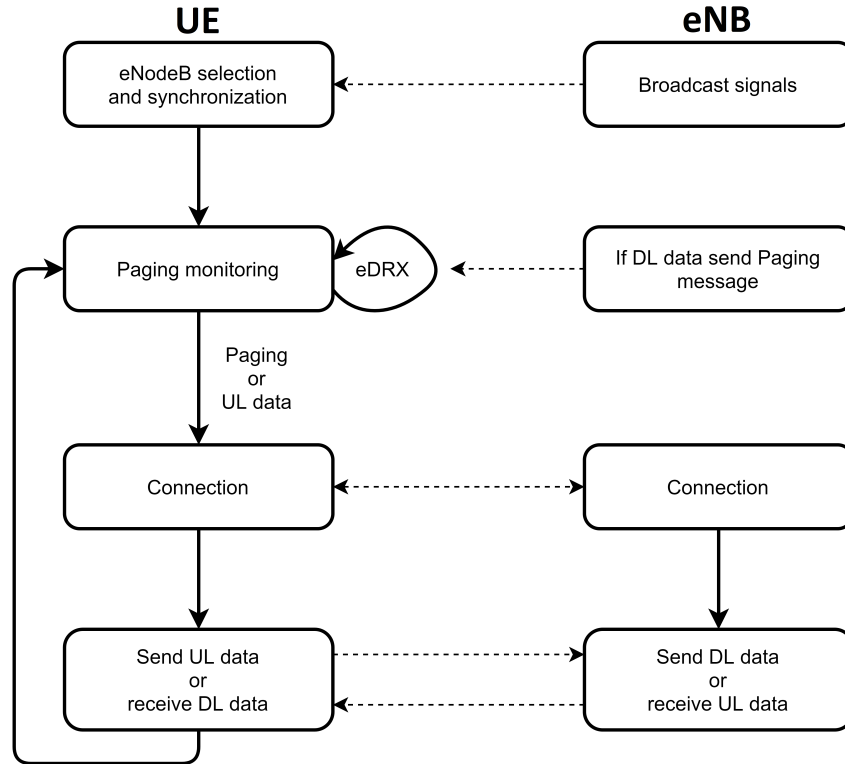


Figure 1.8: Overview of NB-IoT protocol procedures.

to active time, the lower one is the mean power consumption. On the other hand, higher idle time causes an higher latency.

Discontinuous Reception (DRX), extended Discontinuous Reception (eDRX) and Power Saving Mode (PSM) are the main mechanism adopted in NB-IoT for power saving. Three different operation mode are offered in order to fit all possible application requirements. In Figure 1.9 and Figure 1.10 is depicted the current over time behaviour of DRX, eDRX and PSM.

1.4.1 DRX and eDRX

When the eNB needs to connect with a UE, it sends a PM to the UE in the NPDCCH. The PM can be sent only in predetermined occurrences of NPDCCH called Paging Occasions (PO) and a frame containing a PO is called Paging Frame (PF).

Without using any power saving technique, a UE would have to constantly monitor the NPDCCH channel looking for PMs. Although, if DRX is used, the UE monitors the channel with a periodicity multiple of PF. The UE remains active only for the time required to acquire the PF, along with the POs that may be contained

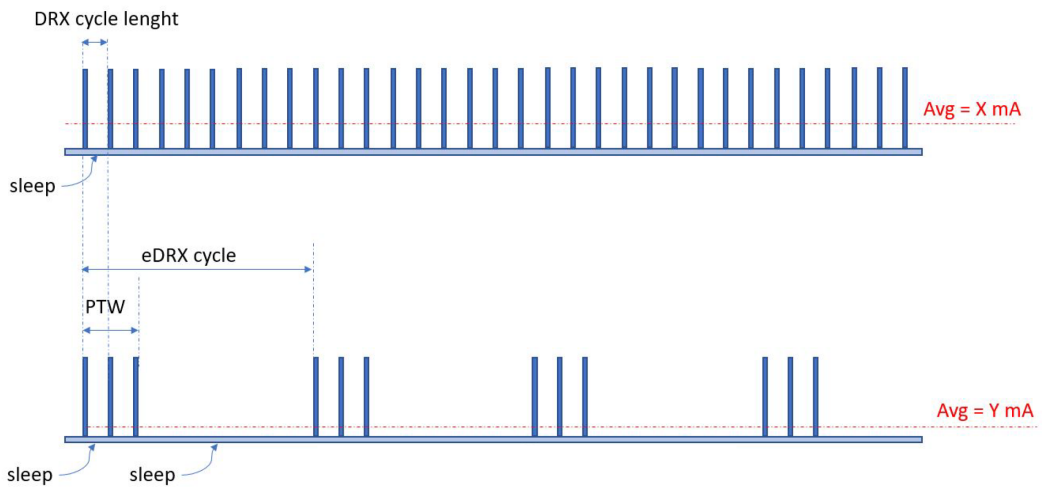


Figure 1.9: DRX and eDRX current profile, [5].

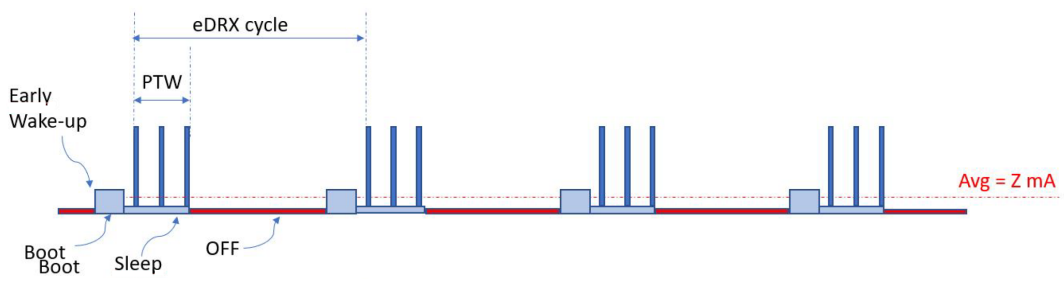


Figure 1.10: PSM current profile, [5].

in the subframes of the PF. With DRX the periodicity can not be very long, in fact it can span from 1.28 seconds to 10.24 seconds. This make DRX useful for applications which need lower latency and have relaxed power consumption requirements.

If eDRX is used, the UE monitors the channel with a periodicity multiple of Paging Hyperframes (PH). With eDRX the periodicity can span from 20.48 seconds to 2.9 hours, making it more flexible. If the idle periods are long, the UE can accumulate an imperfect time synchronization with the eNB, due to the possible local oscillators mismatch. For this reason, the UE remains active for a time window longer than a single PF. The period of time in which the UE remains active is called Paging Time Window (PTW), and it can contain different PFs and thus different POs for the UE, [16].

1.4.2 Power Saving Mode (PSM)

For some applications with very relaxed requirements on latency, the mean power consumption can be further reduced by the means of the power saving mode. In PSM the UE is essentially switched off, with only its real time clock running for keeping track of time and scheduled idle mode events like the Tracking Area Update (TAU) timer. With the TAU procedure the UE informs the network about which cell it camps on, and it is triggered when the TAU timer expires. The device exits PSM once it has uplink data to transmit or at the expiration of the TAU timer to transmit the TAU message. After uplink transmission, the device may enter DRX mode for a configured time, to monitor PO, enabling mobile terminated reachability.

With PSM some UE idle functions are not available. In addition, at every wake-up the UE has to boot-up from scratch, bringing to an high power consuming phase (Figure 1.10). For this reason, its mean power consumption is lower to the one of eDRX only in case of very long sleep periods, [16].

1.5 Downlink Synchronization

As shown in Figure 1.11 the downlink synchronization procedure can be divided in the following steps:

- UE power on.
- NPSS searching identify the presence of an NB-IoT cell.

- Time and frequency synchronization by means of the NPSS in order to identify the carrier frequency and the subframe structure within a frame. The PCID and the three least significant bits of the System Frame Number (SFN) are identified by using the NSSS.
- MIB-NB acquisition to identify the complete SFN and to resolve the frequency raster offset. MIB-NB further provides information concerning how the SIB-NB is transmitted. The SIB-NB is acquired in order to identify the complete SFN, tracking area, and cell identity and to prepare for verification of the cell suitability.
- NPDCCH monitoring to receive PM, ready to start the connection procedure.

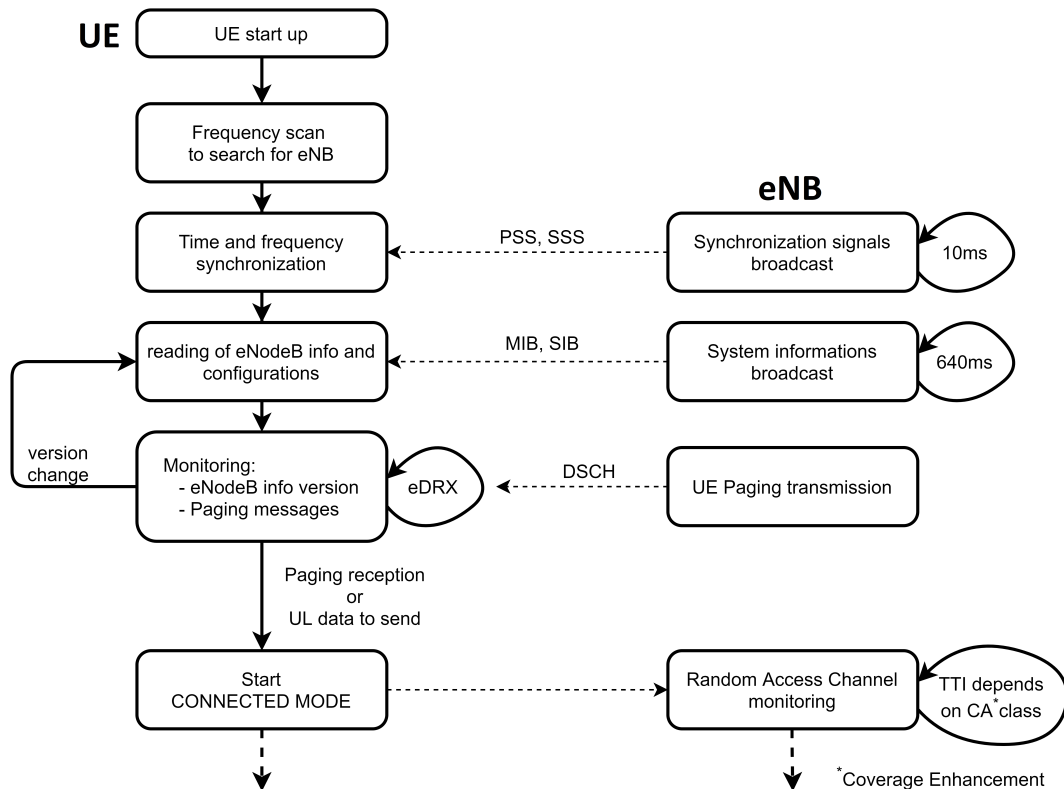


Figure 1.11: Downlink Synchronization procedure.

1.5.1 NPSS: Time and Frequency Synchronization

Due to the limited accuracy of the UE oscillator, the device can accumulate a large frequency shift that can be as much as 20 ppm (e.g., 18 kHz in a 900 MHz band).

Therefore, the NPSS needs to be designed to be detectable even with a very large frequency offset. For this reason, NPSS is generated as a hierarchical sequence based on a base sequence p and a binary cover code c . The base sequence p is a frequency-domain Zadoff-Chu (ZC) sequence, [17].

As depicted in Figure 1.12, NPSS is transmitted in subframe number 5 of every frame, thus by detecting the time instant of NPSS the UE can synchronize with the subframe number of the frame. Once the device has acquired time synchronization, it can use the subsequent NPSS signals to estimate the Carrier Frequency Offset (CFO).

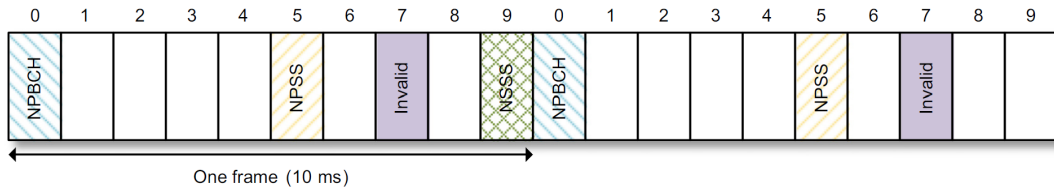


Figure 1.12: NPSS and NSSS frame time occurrence, [1].

A possible method to extract the time delay and the CFO is shown in Figure 1.13. It is useful to accumulate detection metrics over many NPSS subframes in coverage-limited conditions. For this reason, the first step for NPSS detection is to perform the autocorrelation between some NPSS repetition, to gain a coarse subframe timing and fractional CFO. Exploiting this information, it is possible to gain fine subframe timing and integer frequency offset by performing the cross-correlation between the incoming NPSS signal and the known NPSS sequence, [18].

1.5.2 NSSS: PCID and Initial Frame Synchronization

NB-IoT supports 504 unique physical cell identities and there is a different NPSS sequence for every PCID. Thus, the cell PCID can be determined by correctly decoding the NSSS. In addition, NSSS is transmitted in subframe 9 in every even-numbered frame and has an 80-ms repetition interval, within which four different NSSS sequences are transmitted. Thus, by determining which of the four NSSS sequences has been received, the UE understands the frame number of the NSSS in the 80-ms time interval. Thus it can reconstruct the three less significant bits of the SFN, [1].

In a cell, all the NSSS transmissions share the same binary scrambling sequence and extended ZC sequence, in fact they are determined by the cell identity k . Within an 80-ms NSSS repetition interval, the four occurrences of NSSS are differentiated

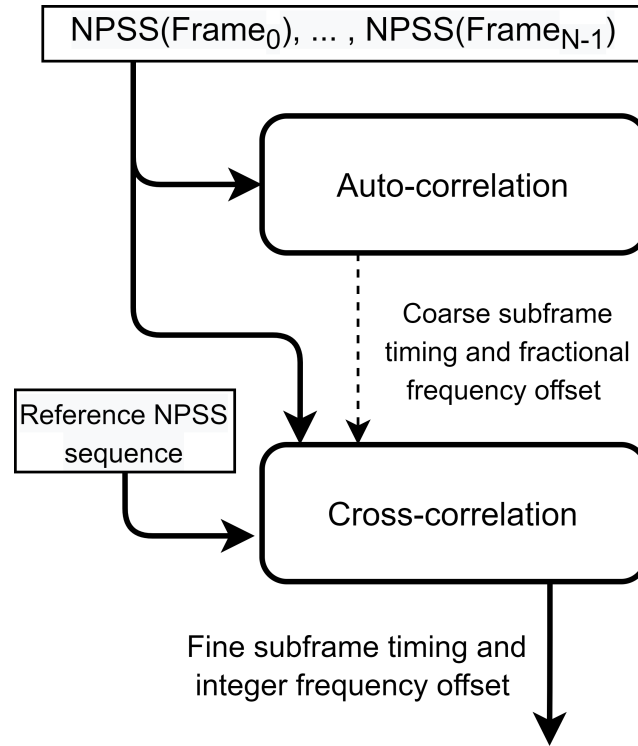


Figure 1.13: NPSS detection method.

by a phase shift.

A straightforward NSSS detection algorithm is to cross-correlate all the NSSS hypotheses with the received NSSS and take the one that have the higher correlation, [19]. This allows to identify the PCID and part of the SFN associated to the decoded hypotheses. As for NPSS, in coverage-limited condition, NSSS detection may rely on accumulating detection metrics over multiple NSSS repetition intervals. An illustration of this procedure is shown in Figure 1.14.

1.6 Random Access Procedure

The Random Access (RA) procedure is the procedure a UE initiates to connect to an eNB. It can be initiated by the UE itself, or by an order from the eNB through NPDCCH. The aim of a UE performing RA procedure is to achieve uplink Synchronization, obtain an uplink grant to request the connection to the eNB and finally establish connection. RA procedure relies on the exchange of four messages, Msg1, Msg2, Msg3, and Msg4, as shown in Figure 1.15, [1].

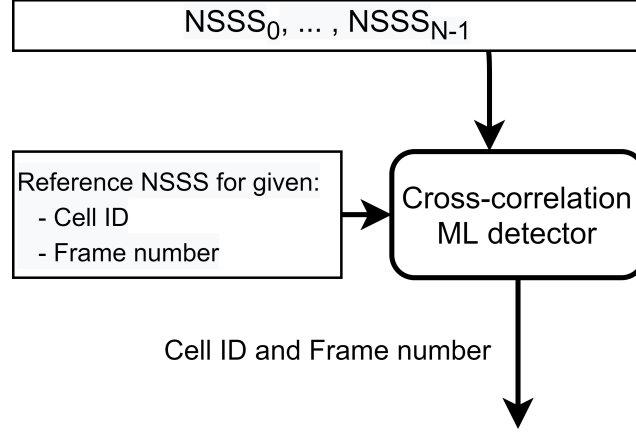


Figure 1.14: NSSS detection method.

Msg1 is the RA Preamble (RAP), it is sent by the UE in NPRACH to initiate the RA procedure and for Time of Arrival (ToA) estimation. If the base station detects a RAP, it sends back a RA Response (RAR) in Msg2. The RAR contains the Timing Advance (TA) parameter, along with the scheduling information used by the UE to transmit the request to connect, known as Msg3. In Msg3 the UE includes its identity as well as scheduling request. Finally, with Msg4, the connection setup message, the eNB resolves any contention that can arise from multiple UE transmitting the same preamble. The connection procedure closes when the UE acknowledges the reception of Msg4, [12].

1.6.1 Random Access Preamble

The network can configure up to three NPRACH resource configurations in a cell, to serve the UEs in different coverage classes which experience different channel conditions. Each NPRACH configuration is associated to a different class of preambles and repetition values. In order to estimate its coverage class, the UE measures its downlink received signal power. Afterwards, it transmits the RAP in the NPRACH resources configured for its estimated coverage level.

NPRACH preambles use single-tone transmission with frequency hopping. A preamble symbol group consists of a CP and multiple symbols, and a preamble repetition unit consists of multiple symbol groups. The three NPRACH formats available in NB-IoT are described in Table 1.1. As shown, the symbol group for Format 0 and Format 1 consist of a CP plus five single-tone symbols of tone frequency $n\Delta f_{NPRACH}$, where n is fixed within a symbol group and Δf_{NPRACH} is the

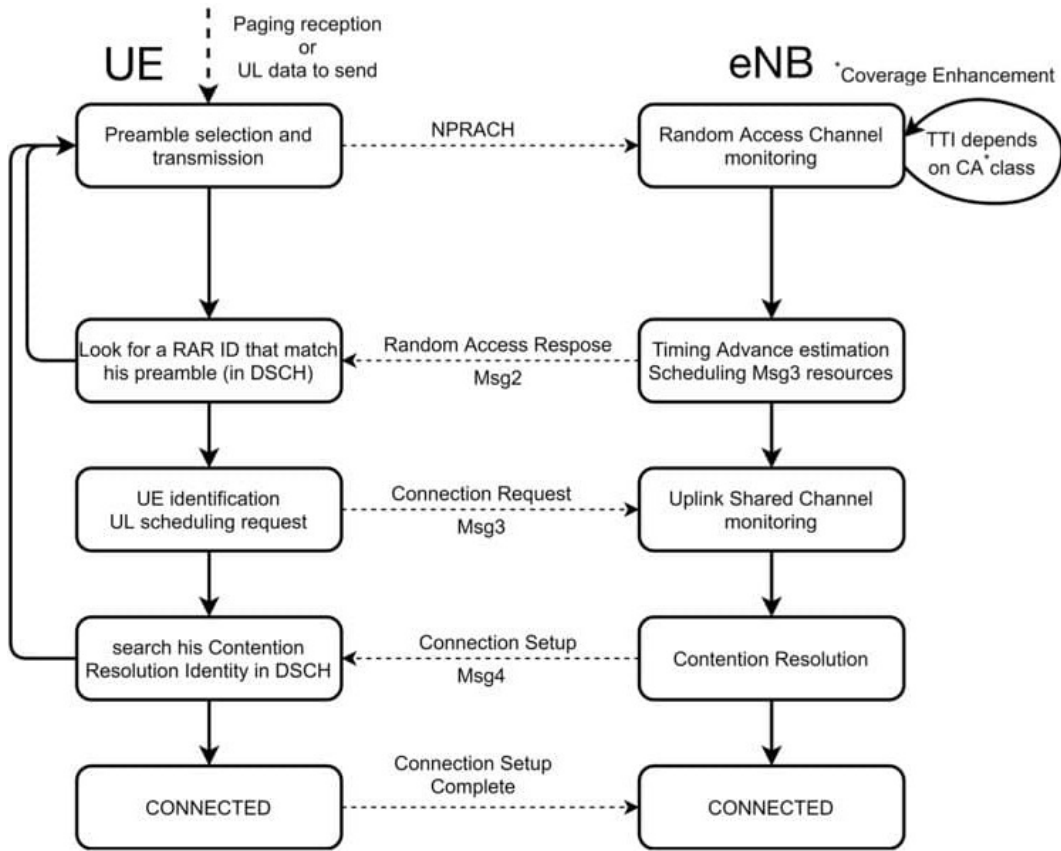


Figure 1.15: Connection Procedure.

tone spacing of 3.75 KHz. Hence, The resulting NPRACH symbol group consists of a continuous phase sinusoidal waveform of baseband frequency $n\Delta f_{NPRACH}$. The same structure holds for Format 2, but with only three single-tone symbols and $\Delta f_{NPRACH} = 1.25$ KHz.

<i>Formats</i>	<i>CP duration</i>	<i>Symbols number</i>	<i>Tone spacing</i>	<i>Repetition unit</i>
Format 0	66.7 μs	5	3.75 KHz	4 symbol groups
Format 1	266.67 μs	5	3.75 KHz	4 symbol groups
Format 2	800 μs	3	1.25 KHz	6 symbol groups

Table 1.1: NPRACH formats characteristics.

NPRACH formats are designed with three different numerologies supporting the different coverage classes they are associated with. For example, format 0 and format

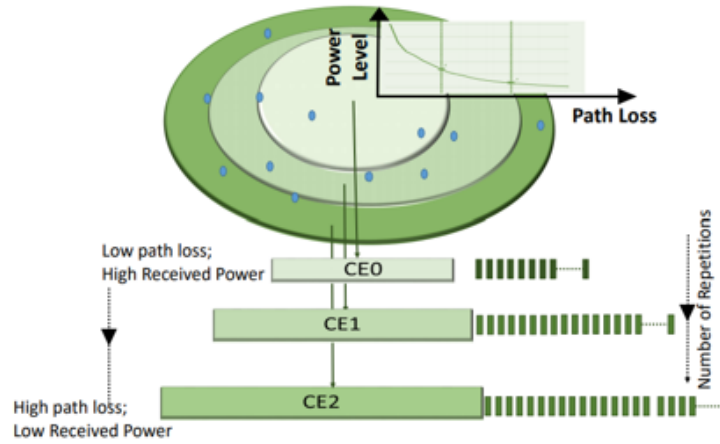


Figure 1.16: Coverage classes, [6].

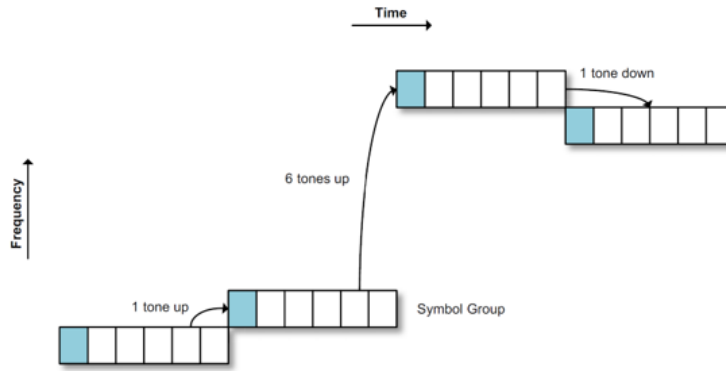


Figure 1.17: Symbol group and frequency hopping pattern, [1].

1 supports a cell radii up to at least 10 and 40 km, respectively. Whereas format 2 supports a cell radius up to 120 Km.

The hopping pattern design is a prominent feature of NPRACH. It consists of both inner layer fixed size hopping and outer layer pseudo-random hopping. In fact, the frequency hopping starting point is chosen randomly but then the hopping follows a fixed pattern. As depicted in Figure 1.17, there are two levels of subcarrier hopping. The first is used between the first and the second and between the third and the fourth symbol groups. In this case it follows a single-subcarrier hopping with a mirrored behaviour between the first couple and the other. The second level of hopping is a 6-subcarrier hopping and it is used between the second and the third symbol groups.

The rationale behind NPRACH hopping pattern design is twofold. Firstly, it creates a set of NPRACH preambles, within a repetition unit, which are orthogonal

and which the UE can use to present itself to the network. The UE randomly selects the RA preamble between the ones associated to its coverage class, then it transmits the RAP in a NPRACH radio resource. Preamble collision occurs if two or more UEs choose the same RAP and the same NPRACH radio resource.

Secondly, the RA preamble is used at the eNB side to estimate the ToA. With hopping, the phases vary across symbol groups. Therefore, the BS can estimate ToA by processing the phases of the received symbols. The maximum ToA Value that can be estimated decreases increasing the hops size. Whereas, the precision of the estimation increases at lower hops size. In fact, the two levels of frequency hopping are introduced to tackle this existing design tradeoff between ToA estimation range and accuracy when choosing the frequency hopping steps. In fact, single-subcarrier hopping ensures a large enough ToA estimation range to meet NB-IoT target cell sizes, while six-subcarrier and pseudo random hopping improve ToA estimation accuracy.

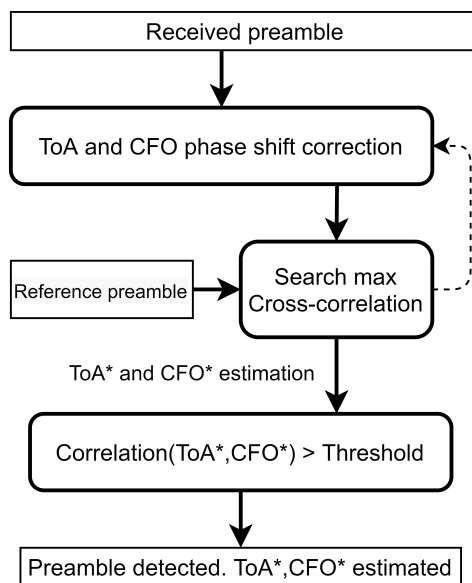


Figure 1.18: preamble detection method.

At eNB side, the preamble has not only a time offset but also a frequency offset. Therefore, the preamble detection algorithm (Figure 1.18) must jointly estimate the phase shifts due to ToA and CFO. The estimate is performed recursively correcting the received symbols with hypothesis (ToA^H, CFO^H) and selecting the one hypothesis that yields the maximum correlation between the received symbols and

the reference preamble. Afterwards, assuming the estimate (ToA^*, CFO^*) has been obtained, the presence of the preamble is determined through the maximum correlation value. If the correlation result exceeds a predetermined threshold[20], the BS declares the presence of the preamble; otherwise, the BS declares that the preamble is not present.

1.7 Uplink/Downlink Transmission Procedure

In this Section, we describe how the procedures for uplink and downlink transmissions work. The data exchange between UE and eNB is coordinated by the scheduling information provided by the network. When the eNB needs to schedule a device, it sends a Downlink Control Information (DCI) addressed to the device through NPDCCH. The DCI contains information about frequency and time resource allocation and information needed for the Hybrid Automatic Repeat Request (HARQ) process. Afterwards, the UE uses this information to transmit or receive data in the scheduled radio resources. Uplink and downlink data transmission procedure are summarized in Figure 1.19 and Figure 1.20 and are detailed in the following Sections, [21].

1.7.1 Uplink Transmission Procedure

For uplink data transmissions, is required a minimum 8 ms time gap between the last DCI subframe and the first scheduled NPUSCH subframe. This relaxed time scheduling allows the device to decode the DCI and to switch the RF from reception to transmission mode. After being scheduled, the UE transmits its uplink data on the NPUSCH in the scheduled radio resource. Subsequently, the UE has another time gap of at least 3 ms allowing the device to switch from transmission to reception mode and be ready to monitor the next paging occasion in NPDCCH. For what concerns uplink transmission, the HARQ process is implemented through an implicit acknowledgement. If the New Data Indicator (NDI) is toggled, the device treats it as an acknowledgement of the previous transmission, otherwise the device repeats the last transmission. An example is shown in Figure 1.21.

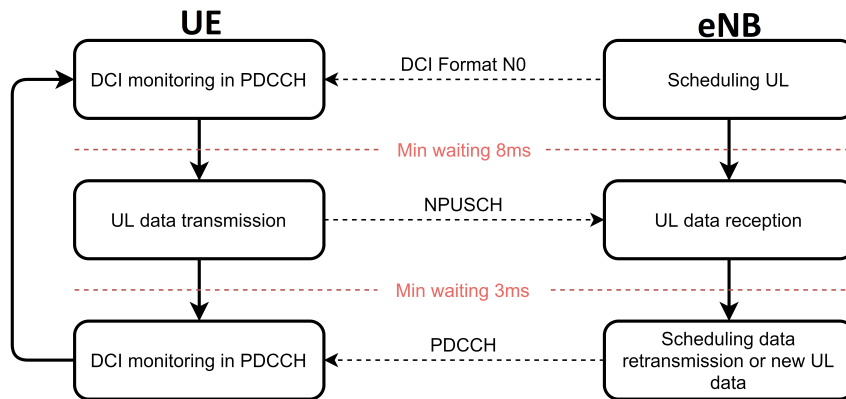


Figure 1.19: Uplink Transmission Procedure.

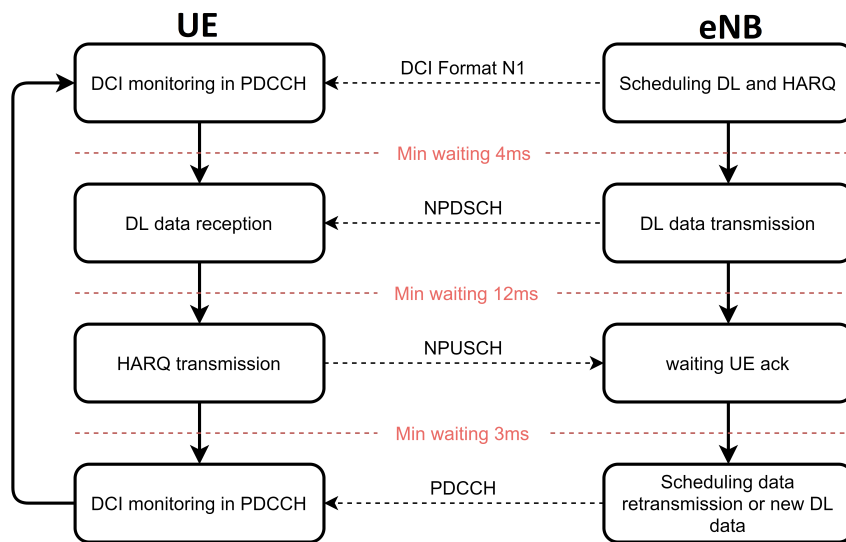


Figure 1.20: Downlink Transmission Procedure.

1.7.2 Downlink Transmission Procedure

Differently from the uplink case, in the downlink the minimum time gap between the last DCI subframe and the first scheduled NPDSCH subframe is only 4 ms. In fact, in downlink there is no need for the device to switch from receive to transmit mode between finishing receiving the DCI and starting the NPDSCH reception. After the scheduling information reception, the UE listens the NPDSCH in the scheduled radio resources. Subsequently, the UE must reply with an HARQ message to acknowledge the downlink reception. Thus, in downlink, the scheduler also needs to schedule NPUSCH Format 2 resources for the signalling of HARQ feedback. In this case, a time gap of minimum 12 ms is defined between the ending subframe of scheduled

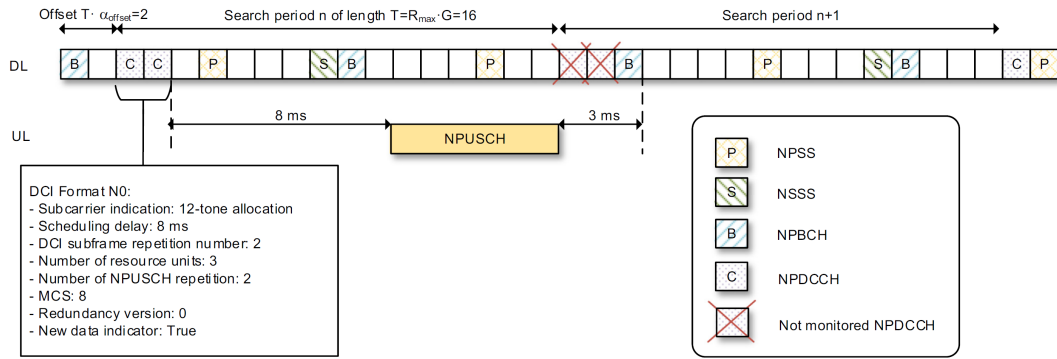


Figure 1.21: Example of uplink transmission scheduling.

NPDSCH and the starting slot of NPUSCH ensuring sufficient time for the device for decoding information and for switching from reception to transmission. For the same reason, a further time gap of 3 ms is introduced between the HARQ transmission and the subsequent NPDCCH paging occasion. An example is shown in Figure 1.21.

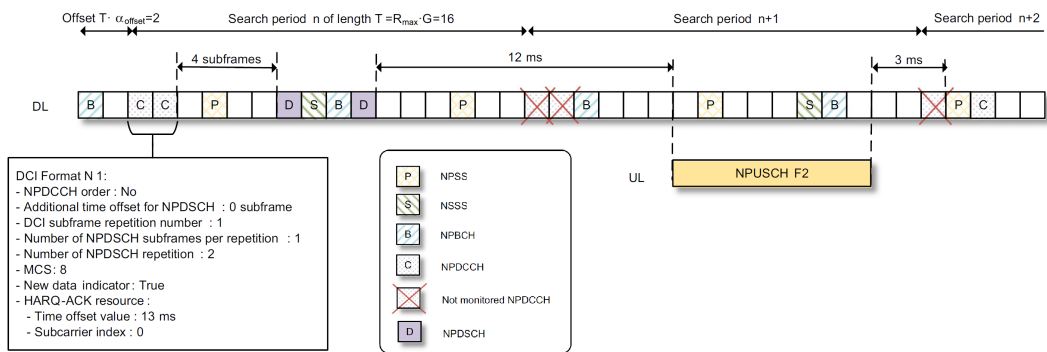


Figure 1.22: Example of downlink transmission scheduling.

Chapter 2

Satellite NB-IoT Service Provision

NB-IoT deployment is going to satisfy most of the requirements for a wide range of IoT application in urban areas. On the other hand, there are many IoT scenarios for which terrestrial network deployment is unfeasible or not economically profitable. For these applications, satellite communications (SatCom) have the potential to play an important role. Notably three main areas have been identified in [9]:

- Smart objects for infrastructure or environmental monitoring are often in remote locations or they are spread over a wide geographical area (e.g. mid desert pipeline or sea sensors). In these cases, SatCom provides a more cost-effective solution with respect to other terrestrial technologies.
- In the context of critical IoT applications, SatCom can play an important role since reliability is a fundamental requirement.
- Since IoT is characterized by low data rate requirement, satellite operators can find in IoT a profitable way to reuse their low bandwidth satellite infrastructures, [22].

SatCom solutions have been usually designed for specific tasks and services, without cooperation with terrestrial networks. However, in order to serve the plethora of new IoT use cases and services, a new synergy among these two systems must be established. Recognizing its importance, 3GPP is supporting the interoperability of Non Terrestrial Networks (NTN) and terrestrial communication system since Release 15, [23].

This Chapter aims at analyzing the feasibility of utilization of NB-IoT terrestrial standard on a satellite communication channel. The main issues are investigated, and possible solutions are proposed. In particular, some possible architectures of a SatCom system are presented and a reference scenario for the NB-IoT case is selected. Then, the impact of Doppler shift and long propagation delays on the NB-IoT protocol are investigated.

2.1 System Architecture

In this Section two possible system architectures are presented. Thus, in order to make the discussion clear, the most important architecture components are presented: i) the Core Network (CN) is the central part of the overall mobile network and is responsible to manage some network level procedures of the protocol; ii) the Gateway (GW) is the on-ground transceiver that connects the satellite to the core network; iii) the Satellite (Sat) is the spacecraft responsible to connect the GW with the UEs.

In the direct access scenarios shown in Figure 2.1 and 2.2 the user link (between Sat and UEs) directly involves the satellite and the on-ground UEs by means of the NB-IoT air interface. This air interface is specifically designed for terrestrial systems and, thus, it is fundamental to assess the impact of the satellite channel impairments on both Physical (PHY) and Medium Access Control (MAC) layer procedures. With respect to the feeder link (between Sat and GW), the air interface to be implemented depends on the type of satellite payload¹. Indeed, in the next two Sections transparent and regenerative payloads will be presented.

2.1.1 Transparent Payload

As for the transparent payload satellite, the system eNB is conceptually located at the GW providing the connection towards the CN and the public data network. More specifically, the signals received by the satellite user beams are amplified, filtered, and translated infrequency; then, the signals are retransmitted toward the terrestrial gateway through the feeder link on dedicated frequency band. An opposite path is

¹The payload is the part of the satellite spacecraft dedicated to telecommunication purposes. Considering the transparent payload, it includes the antenna, low and high power amplifiers, filters and frequency converters. Furthermore, the regenerative payload includes also the demodulator, the modulator and computing capability in order to perform some protocol functions also at the satellite.

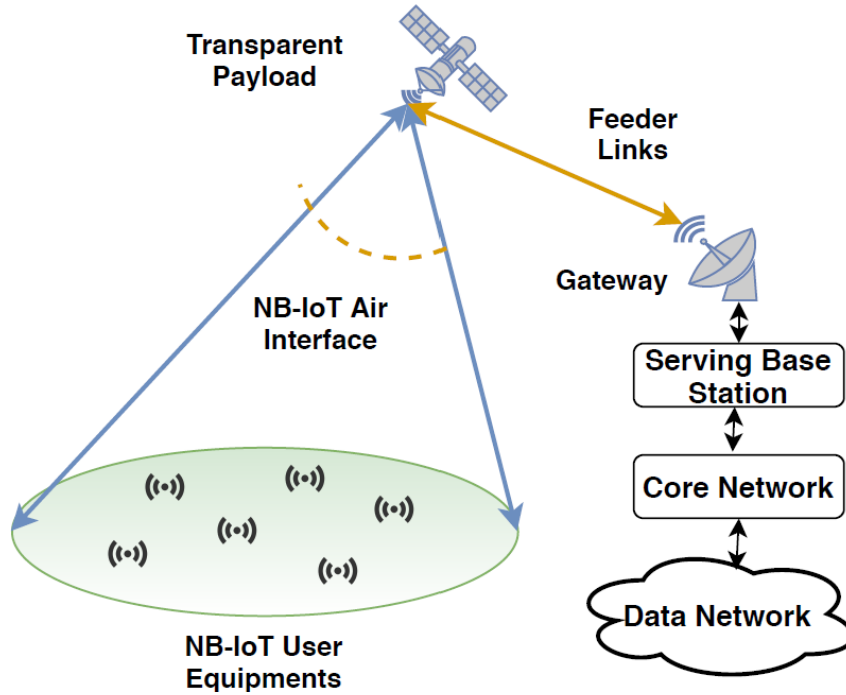


Figure 2.1: NB-IoT NTN with transparent payload, [7].

followed by the signals flowing from the gateway to the UE. The described system architecture is shown in Figure 2.1. In this architecture, the feeder link air interface is again provided by the terrestrial NB-IoT, thus, the impact of the different satellite channel impairments has to be assessed also in this case.

2.1.2 Regenerative Payload

As for the regenerative payload satellite, the system eNB is implemented on the satellite, while the GW simply provides the connection towards the CN and public data network. In this case, all the eNB functions are performed in the satellite, thus, only the user link must be implemented using the NB-IoT air interface. On the contrary, the feeder link can be implemented relying on any suitable air interface.

This architecture has higher cost compared to the transparent payload since it is clearly more complex. However, it significantly reduce the satellite channel effects on the NB-IoT protocol. In fact, the physical and MAC procedures can be directly terminated on the on-board eNB instead of requiring to go down to the GW, thus the propagation delays are significantly reduced.

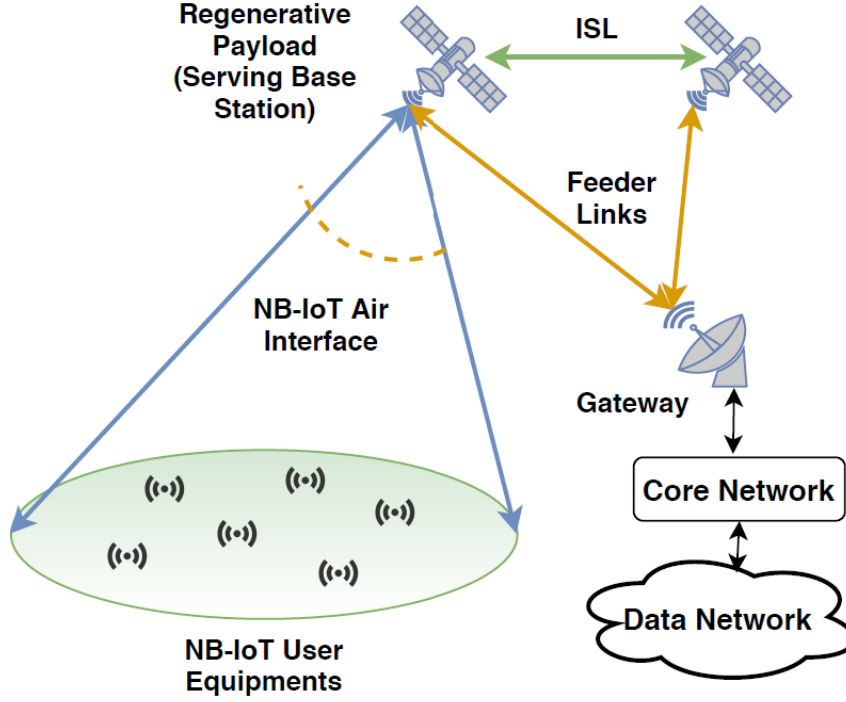


Figure 2.2: NB-IoT NTN with regenerative payload, [7].

2.2 Orbits

In this Section the different types of satellite orbits and constellations are presented. 3GPP has focused on Geostationary Earth Orbit (GEO) and Low Earth Orbit (LEO) constellations for the deployment of NB-IoT. A third deployment possibility is the High-Altitude Platform Station (HAPS). In this context, it consists of an aircraft, e.g. balloons or airplanes, that operates in the atmosphere at high altitudes for extended periods of time, in order to provide the NB-IoT service. However, the channel impairments introduced by the HAPS deployment are far less severe compared to GEO and LEO. Therefore, only GEO and LEO orbits are tackled in the following Sections.

2.2.1 Geostationary Orbit

A geosynchronous orbit (Figure 2.3) is characterized by an orbital period of 24 hours, meaning that the satellite movement along its orbit is synchronous with the Earth's rotation. When a geosynchronous satellite is placed on the equatorial plane, at altitude of 35.787 Km, the orbit is said geostationary. In this case, an observer from earth sees the geostationary satellite in a fixed position in the sky. This equatorial

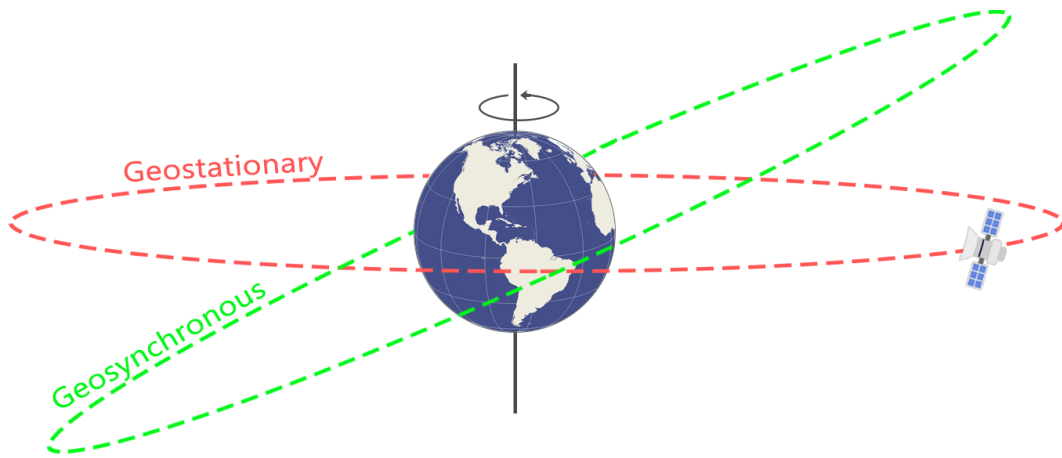


Figure 2.3: Geosynchronous and geostationary orbits.

geosynchronous orbit is very crowded due to its unique characteristics. Thus, in order to avoid interference between adjacent GEO satellites, each satellite is assigned a well delimited orbital slot, which corresponds to a distinct longitudinal position.

2.2.2 Low Earth Orbit

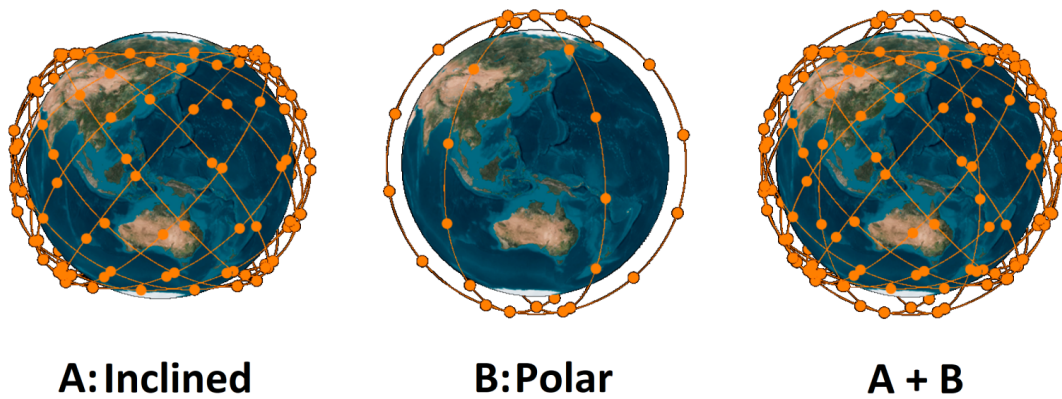


Figure 2.4: LEO at different inclinations.

LEO satellites altitudes range between 500 and 2000 km, involving orbital periods between 94 and 127 minutes, [24]. The orbit inclination is the angle of the orbit in relation to Earth's equator. A satellite that orbits directly above the equator has zero inclination. If a satellite orbits from the geographic north pole to the south pole, its inclination is 90 degrees. LEO satellites can be deployed at any inclination angle as seen in Figure 2.4. However, the deployment of a satellite at inclination value of either 28.5 degrees or 57 degrees can be easier, due to typical launch locations, [25].

LEO orbits are usually exploited for earth observation and communication satellites. For what concerns the satellite footprint, two types of deployment have been considered by 3GPP: Earth-moving beams and Earth-fixed beams. In the former, as depicted in Figure 2.5a, the satellite beams follow the satellite movement along the orbit, implying a coverage of a fixed point on Earth for just a few seconds. In the latter, as depicted in Figure 2.5b, the satellite realizes spotbeams that remain fixed on Earth².

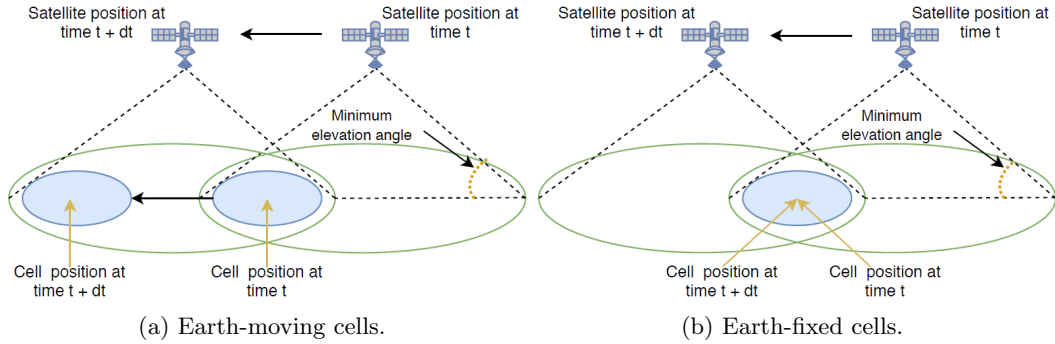


Figure 2.5: LEO satellite footprint typology, [7].

2.2.3 GEO and LEO Scenarios Comparison

Making use of GEO it is possible to obtain a full earth coverage, polar region excluded, deploying only three satellites and gateways. By contrast, LEO presents a totally different scenario. In this case, in order to provide real-time global Earth coverage, the number of satellites and gateways required is much larger, and depends on the chosen orbit and the surface covered by the satellite antenna. In order to decrease the deployment and operational costs of the system one can reduce the number of LEO satellites selecting an inclined orbit. This ensures good coverage of the Earth after a given number of spacecraft revolutions; thus, it is a viable solution only when the message delivery latency is not an issue. Moreover, the number of terrestrial gateways can be reduced to one using a regenerative payload (Figure 2.2), hence deploying all eNB functionalities on the satellite.

LEO is characterized by high Doppler shift with compared to GEO. However, LEO constellations provide reduced round trip time compared to GEO, which, as discussed in section 2.5, is of relevance in NB-IoT protocol. Moreover, LEO is

²The satellite can steer the spotbeams by tilting its antenna or by the means of attitude modifications.

characterized by a time variant geometry between the satellite and the UE that increases the probability of instantaneous Line of Sight (LoS) condition compared to GEO, allowing information delivery. On the other hand, LEO can cause temporary link unavailability causing an increase in the data delivery time.

2.3 Reference Scenario

To analyze the implementation feasibility of the NB-IoT terrestrial standard in a satellite channel, a reference scenario must be defined.

As aforementioned, not only, satellite links introduce very large propagation delays compared to terrestrial links, but also, GEO introduces larger delay than LEO. Since NB-IoT terrestrial technology is sensitive to high propagation delays, in the following we focus on LEO satellites, considering an altitude between $h_{sat} = 600km$ and $h_{sat} = 1500km$. For what concerns the operational frequency, it is constraint by the NB-IoT standard in the S-Band, i.e., 2170-2200 MHz downlink and 1980-2010 MHz uplink.

In terms of system architecture, the reference scenario is defined by the following assumptions: i) the on-ground UEs are directly connected to the satellite; ii) the satellite is assumed to be transparent and to provide backhaul connection between the GW and the on-ground UEs; iii) the satellite provides coverage through Earth-moving beams; iv) the GW is connected to the satellite through an ideal feeder link, providing access to the terrestrial CN. The defined reference scenario is shown in Figure 2.1.

In the next Sections the main satellite channel impairments introduced by this reference scenario are analyzed.

2.4 Doppler

The Doppler shift consists in the offset in the carrier frequency due to the relative motion between the transmitter and the receiver. In satellite communications, the Doppler shift can be caused by the user terminals' mobility on ground, but it is mainly due to the satellite movement on its orbit.

A closed-form expression for the Doppler shift as a function of the satellite orbital velocity and the elevation angle θ has been defined in [26]:

$$f_d(t) = \frac{f_c \cdot \omega_{sat} \cdot R_E \cdot \cos(\theta_{UE}(t))}{c} \quad (2.1)$$

where $\omega_{sat} = \sqrt{GM_E/(R_E + h_{SAT})^3}$ is the satellite orbital velocity, R_E is the Earth radius, $G = 6.67 \cdot 10^{11} Nm^2/kg^2$ the Gravitational constant, and $M_E = 5.98 \cdot 10^{24}$ Kg the Earth mass.

When considering GEO systems serving fixed on-ground UEs, the relative velocity between satellite and UEs is negligible, thus the Doppler shift can be assumed to be negligible. Nevertheless, for what concerns the LEO satellites considered in the reference scenario, the orbital speed is high. Thus, the relative velocity between satellite and UEs is often considerable, leading to a Doppler shift which can be significantly higher with compared to Doppler expected in terrestrial systems.

2.4.1 Differential Doppler

In the reference scenario, the Doppler experienced by the i -th user in the DL channel and, viceversa, on the satellite with respect to the i -th user in the UL channel consists of two contributions. It can indeed be described as $fd_i = fd_{common} + \Delta fd_i$, where fd_{common} is the common part of the Doppler experienced by every user in the same footprint while Δfd_i , the differential part, depends on the relative positions of users in the footprint, [8].

The main contributor towards the differential Doppler shift is the change of position along the direction of the satellite movement (x axis), whereas for the perpendicular one (y axes) differential Doppler is negligible. The maximum differential Doppler shift given the cell radius x can be calculated as derived in [27]:

$$\Delta f_d^{MAX} = \left| \frac{f_c \cdot \omega_{sat} \cdot R_E}{c} \cdot (\cos(\theta_{UE1}(t)) - \cos(\theta_{UE2}(t))) \right| \quad (2.2)$$

Considering the DL user link (from Sat to UE), the differential Doppler is not an issue since each UE must compensate its own experienced Doppler fd_i . Indeed, each UE under the same Doppler condition will receive the whole bandwidth of 180 kHz, with negligible effects on the single subcarriers. On the other hand, In the UL user link (from UE to Sat), each UE generates its own SC-FDMA signal, thus the differential Doppler must be compensated such that the frame structure seen by the satellite does not contain overlapping information among subcarriers, [8]. Furthermore, the feeder link (from eNB to Sat and viceversa) can be considered ideal,

without Doppler impairments. This is motivated by noticing that, in this case, the Doppler is applied to the whole signal, so it does not introduce differential Doppler effects. Hence, it can be compensated even at the eNB. Due to the considerations mentioned above, only the effect of Doppler shift in the uplink user link will be tackled.

Since each k -th UE is in a different position on the coverage area, it experiences a different Doppler value at the same time instant, thus, there is a correlation between the users positions and the differential Doppler experienced.

The received baseband signal at the eNB due to the differential Doppler between UEs is given by :

$$y_R = \sum_{k=1}^N x_{UE_k} e^{-j2\pi f_{d_k}(t)t} = e^{-j2\pi f_{d_1}(t)t} \sum_{k=1}^N x_{UE_k} e^{-j2\pi \Delta f_{d_k}(t)t} \quad (2.3)$$

where $f_{d_k}(t) = f_{d_1}(t) + \Delta f_{d_k}(t)$ and f_{d_1} is the Doppler of one user in the cell taken as a reference. The nomenclature adopted in the mathematical formulation can be found in Table 2.1, [8].

<i>Definition</i>	<i>Symbol</i>
Number of nUE in the cell	N
RX baseband signal $nUE_K \rightarrow eNB$	YR
TX baseband signal $nUE_K \rightarrow eNB$	x_{UE_k}
nUEs carr. freq. off. (coomon) w.r.t. eNB	f_{ko}
Differential Frequency Offset pf nUEs	f_{Δ_k}
Freq. off. added by nUE_k loc. osc.	$f_k = f_{ko} + f_{\Delta_k}$
Doppler added at t for k-th user ($Sat \rightarrow nUE$)	$f_{d_k}(t)$
Doppler added at $t + \tau$ for k-th user ($nUE \rightarrow Sat$)	$f_{d_k}(t + \tau)$

Table 2.1: Nomenclature for Doppler analyzes.

Looking at this expression, the common part ($e^{-j2\pi f_{d_1}(t)t}$) can be easily compensated at the eNB relying on the satellite ephemeris data, while the differential

Doppler amongst users must be pre-compensated at each UE to avoid dangerous degradation.

As discussed in 3GPP specifications [28] and [29] about mobile UEs, LTE physical layer is specifically designed to tolerate a Doppler up to 950 Hz, considering a carrier frequency of 2 GHz and a maximum relative speed at 500 km/h. Therefore, since $f_{d_{common}}$ can be compensated at the eNB, it is possible to assume that for a subcarrier spacing of 15 kHz a value of Δf_{di} up to ≈ 950 Hz could be tolerated. Proportionally, for a subcarrier spacing of 3.75 kHz the value of Δf_{di} should be lower than ≈ 240 Hz [9], to fulfill the constraints on Doppler for NB-IoT.

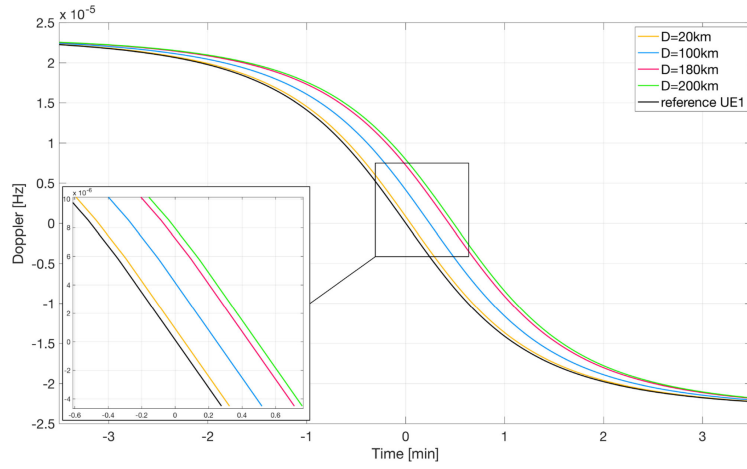
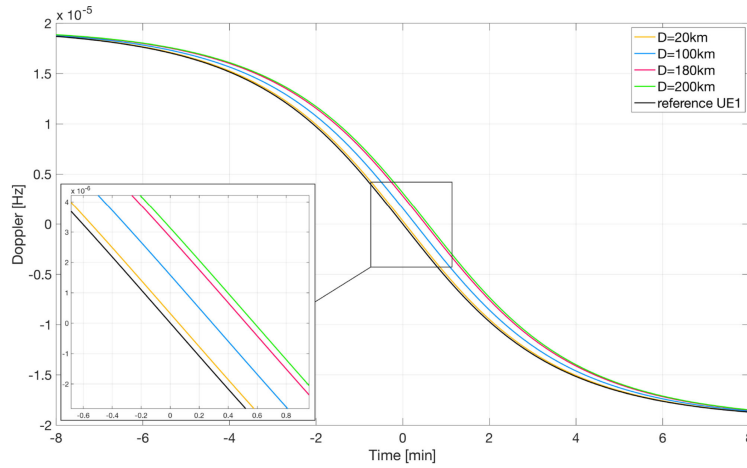
2.4.2 Differential Doppler Assessment

The purpose of this paragraph is to quantify the differential Doppler in worst-case conditions and compare the results with the constraint given by NB-IoT. Simulations have been performed in [8] considering the parameters in Table 2.2. Figures 2.6 and 2.7 show the Doppler behaviour over time for two UEs placed at different distances in the coverage area. The differential Doppler, as seen by the satellite antenna at each timing instant, is the difference between the curve of the considered distance and the reference curve, and it is highlighted in Figure 2.8. It can be noticed that the worst-case differential Doppler increases at higher distances and decreases at higher orbits.

<i>Parameter</i>	<i>Value</i>
Carrier Frequency	2.2 GHz
Satellite altitude range	600-1500 km
Elevation angle	90°
Minimum elevation angle	10°
Reference UEs reciprocal distance	40-200 km

Table 2.2: Simulation Parameters.

It is worth to notice that the differential Doppler values from simulation in Figure 2.8 are compliant with LTE Doppler constraint only for small maximum distances and high orbits. Therefore, the only way to keep the differential Doppler shift under LTE Doppler constraints, without modifying the existing standard, is

Figure 2.6: Doppler curves of reference UEs, $h_{SAT} = 600km$, [8].Figure 2.7: Doppler curves of reference UEs, $h_{SAT} = 1500km$, [8].

to reduce the cell size. As mentioned in the last Section, the differential Doppler depends only on the UE distance on the x-axis, therefore it can be worth to consider ellipsoid cells with the mayor axis in the y direction.

The limitations on the cell radius and orbits can become very stringent without modifying the existing standard. Thus, the design of some technique to reduce the Doppler down to the limit reported in the previous section can be beneficial.

2.5 Doppler Mitigation Techniques

To mitigate the Doppler effect using a pre-compensation procedure each UE must know the instantaneous Doppler that he generates at the satellite antenna. The

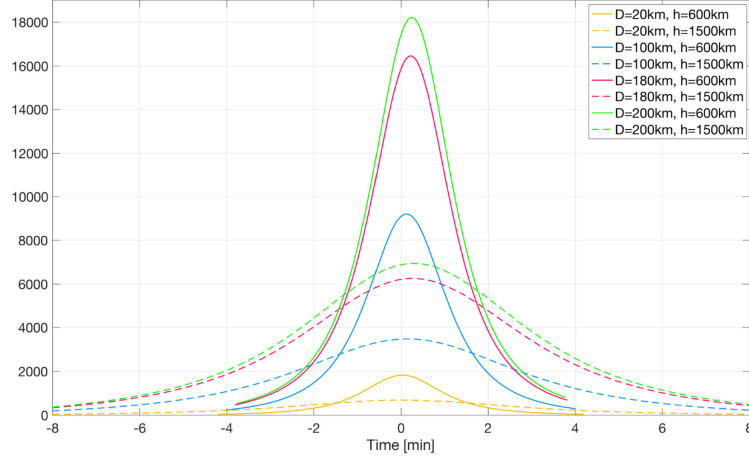


Figure 2.8: Doppler shift analysis, [8].

carrier error is generated by the channel and it is not a straightforward information to obtain, thus some estimation technique should be adopted. In the following Sections, a non exhaustive set of estimation techniques, selected after a state of the art analysis, is proposed.

2.5.1 Frequency Advance

A useful technique to be considered for Doppler mitigation is the so called frequency advance. It allows to estimate the frequency offset in the forward link and then reuse it to reduce frequency offset in the reverse link. In general, this technique is not designed for differential Doppler mitigation, but it can be adapted to this scope. Indeed, in [9] is proposed a method based on the estimation of the Doppler experienced in UL based on the DL channel.

It is demonstrated that if the UL transmission occurs within a sufficiently small time interval (τ_k) after the offset has been estimated on the DL signal, the Doppler can be assumed almost constant. In this case, using the offset estimated on the DL channel with opposite sign in the UL transmission, the undesired differential Doppler can be mitigated.

In order to evaluate the maximum value for τ_k , it is necessary to compute the τ_k value that corresponds to a residual differential Doppler compliant with the NB-IoT maximum Doppler requirement. The maximum allowed values for τ_k derived in [9] are reported in Table 2.3. The results of the simulation are reported for satellite altitude value ranging from 300 to 1200 km and considering the worst case scenario. The residual differential Doppler over time (for $\tau_k = 1337ms$) is depicted in Figure

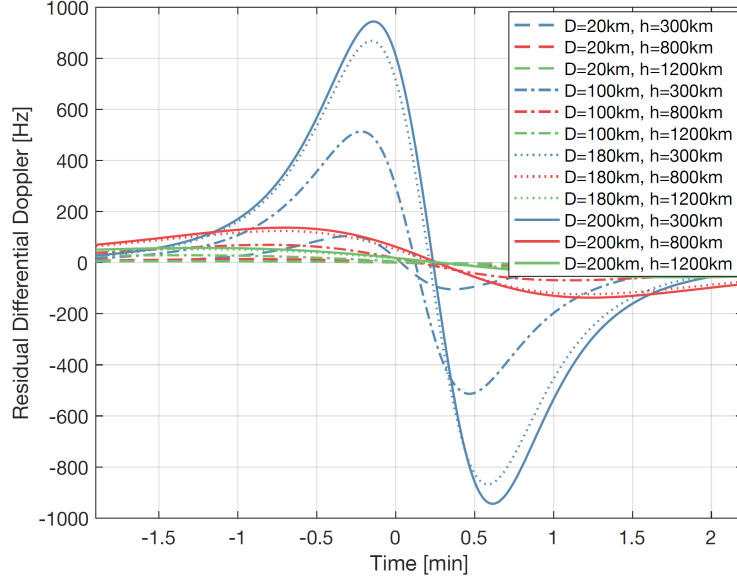


Figure 2.9: Residual differential Doppler, [9].

2.9 and it can be seen that the Doppler requirements are respected. Finally, in [9] the typical values of τ_k for an hypothetical system are assessed, concluding that in case of 100% gateway availability τ_k will never exceed its maximum values.

h_{SAT}	$\tau_{MAX} \Delta f_{sc} = 15 \text{ kHz}$	$\tau_{MAX} \Delta f_{sc} = 3.75 \text{ kHz}$
300 km	1337 ms	303 ms
800 km	9378 ms	2356 ms
1200 km	22511 ms	5686 ms

Table 2.3: Maximum values for τ_k , [9].

2.5.2 CP Based and Map Based Estimation

In this Section, two methods for the Doppler estimation in OFDM-based waveforms are reported, since they can be useful for the estimation of the Doppler experienced by each user.

In the first method, the Doppler is estimated by using a cyclic prefix based algorithm in [30]. This method is shown to have good performance in AWGN channels while it suffers in multipath channels, [31]. In addition, the maximum Doppler shift

that can be estimated by this CP-based algorithm is half of the subcarrier spacing.

In the second method, a MAP Doppler estimator presented in [32], a two step approach is used. In the first step, the algorithm performs a first estimation relying on the cyclic prefix. In the second step, the estimation is refined considering the predictable characterization of the Doppler given by the known circular orbit of a LEO satellite. An interesting advantage of the technique is the possibility to work with mobile terminals up to a speed of 500 km/h, while keeping a low MSE for the Doppler shift estimation ($\approx 10^{-5}$ dB).

2.5.3 Position Tracking

As analyzed in [24], a UE may use its Global Navigation Satellite System (GNSS) location information in combination with satellite ephemeris data to compensate for Doppler effects to a high extent. A residual Doppler shift can occur in case of an error in the estimation of the relative position between the UE and the satellite. The difference between the compensated and the actual Doppler shift can be computed from geometrical considerations and in order to keep the residual Doppler shift below 950 Hz, it is possible to conclude that the position error must be smaller than 4 km, [26].

Even though GNSS integration is compatible with the current NB-IoT devices, a GNSS receiver can drain part of the battery life of the UE, as well as increase the device cost. A straightforward solution for this high power consumption, would be to periodically disable the GNSS exploiting the latest position information for the differential Doppler estimation. This method decreases the energy consumption, but it impacts on the accuracy of the estimation.

Nevertheless, while this solution based on the UEs position can be applied on the existing NB-IoT devices, an additional algorithm, like the aforementioned ones, would result in an additional core to be included in the standard chip.

2.5.4 Resource Allocation Strategy

In [33], in order to limit the differential Doppler shift up to a level supported by the standard, a resource allocation strategy is proposed. Basically, the method consists in splitting the coverage area in smaller regions such that the UEs in each region experience a maximum reciprocal differential Doppler below the allowed threshold. Then, the eNB allows the connection of UEs one region at a time. As a result, the eNB schedules in adjacent time slots only the UEs which have low reciprocal

differential Doppler. Since in message 1 of the RA procedure the transmission is not controlled by the eNB, this solution is exploitable only from message 3 transmission to all the subsequent transmissions.

2.6 Round Trip Time

In satellite communications the propagation delay reaches much larger values with compared to those of terrestrial networks, resulting in possible problem for some protocol procedures. Depending on the type of procedure analyzed, the one-way propagation delay or the Round Trip Time (RTT) shall be considered. Since the signal processing time in a SatCom context can be assumed negligible with respect to the propagation delay, the RTT can be approximated by twice the propagation delay between the transmitter and the receiver. As stated in [8], in the general case in which the transmitter and the receiver are not perfectly aligned, i.e., they have different elevation angles, the overall RTT can be computed as:

$$RTT \approx 2T_{owp} = 2 \frac{d_{GW-Sat}(\theta_{GW}) + d_{Sat-UE}(\theta_{UE})}{c} \quad (2.4)$$

Where T_{owp} is the one-way propagation delay, d_{GW-Sat} is the gateway-satellite distance as a function of the gateway elevation angle θ_{GW} , d_{Sat-UE} is the satellite-UE distance as a function of the UE elevation angle θ_{UE} , and c the speed of light.

An example of RTT computation has been presented in [8]. The following pessimistic scenario has been considered for the computation. The system GW is assumed to be at $\theta_{GW} = 5^\circ$, elevation angle, while the minimum elevation angle for the UEs is assumed to be $\theta_{UE} = 10^\circ$. The results for the single path distances and the involved delays, considering both the minimum and the maximum satellite altitude of the reference scenario are listed in Table 2.4 and Table 2.5 respectively. Additionally, the results for the GEO scenario are listed in Table 2.6 for comparison. Finally, the one-way propagation delay and the RTT can be obtained, they are shown in Table 2.7.

While in the GEO scenario the propagation delay might be an issue for all procedures, with respect to our reference scenario a case-by-case evaluation of the

<i>Elevation angle</i>	<i>Path</i>	<i>Distance [km]</i>	<i>Delay [ms]</i>
UE: $\theta_{UE} = 10^\circ$	Sat-UE	1932.25	≈ 6.44
GW: $\theta_{GW} = 5^\circ$	Sat-GW	2329.03	≈ 7.76

Table 2.4: Reference LEO scenario: $h_{sat} = 600km$, [8].

<i>Elevation angle</i>	<i>Path</i>	<i>Distance [km]</i>	<i>Delay [ms]</i>
UE: $\theta_{UE} = 10^\circ$	Sat-UE	3647.55	≈ 12.16
GW: $\theta_{GW} = 5^\circ$	Sat-GW	4101.72	≈ 13.67

Table 2.5: Reference LEO scenario: $h_{sat} = 1500km$, [8].

delay impact is needed.

For example, even if the latency constraints in NB-IoT are relaxed, some protocol timers must be taken into account into the investigation. In particular, some timer in the Random Access procedure and Radio Resource Control (RRC) procedures can be incompatible with satellite RTT delays. Furthermore, a long RTT has an impact on the UE battery life because it implies longer wake up period for UEs in order to perform RA procedures and data transmission.

2.7 Differential Propagation Delay

In this Section, the Differential Propagation Delay (DPD) is introduced. If the UEs are located in different positions on the cell, they have a different slant range. Furthermore, this difference in the propagation distance between the UEs yields a difference in the propagation delay. The DPD can be described as $fdel_i = fdel_{common} + \Delta fdel_i$, where $fdel_{common}$ is the common part of the delay experienced by every user in the same footprint while $\Delta fdel_i$, the differential part, depends on the relative positions of users in the footprint. The common part is compensated by the UE in the downlink synchronization procedure, when it acquires time synchronization with the eNB.

Some NB-IoT procedures require that the signals from different UEs arrive at the eNB within a maximum DPD, which can be adapted based on the coverage area. In particular, the maximum cell radius is strictly connected with the timing constraints of TA and RA procedures. In terrestrial systems there is maximum DPD when a

<i>Elevation angle</i>	<i>Path</i>	<i>Distance [km]</i>	<i>Delay [ms]</i>
UE: $\theta_{RN} = 10^\circ$	Sat-RN	40586.07	≈ 135.28
GW: $\theta_{GW} = 5^\circ$	Sat-GW	41126.72	≈ 127.09

Table 2.6: GEO scenario: $h_{sat} = 35786km$, [8].

<i>Scenario</i>	<i>One-way [ms]</i>	<i>RTT [ms]</i>
GEO	≈ 272.37	≈ 544.75
Ref. GEO at $h_{sat} = 600km$	≈ 14.2	≈ 28.4
Ref. GEO at $h_{sat} = 1500km$	≈ 25.83	≈ 51.66

Table 2.7: One-way propagation delay and RTT for the considered scenarios, [8].

UE is located close to the eNB and the other at the cell edge, and it is often not a limiting factor. On the other hand, considering SatCom systems with significantly longer RTT with respect to terrestrial communications, the DPD becomes one of the critical aspects and the cell dimension must be dimensioned according to it.

In our reference scenario, on the user link (UEs \leftrightarrow satellite) each UE transmission has a different propagation paths and, thus, introduce a differential delay. Differently, the feeder link (satellite \leftrightarrow eNB) is common to all UEs and, thus, it does not introduce any DPD in the signal propagation. For this reason, only the user link is considered in the following.

To compute the maximum DPD of a specific cell with radius x , the worst-case scenario in which two UEs are located at the cell edge on opposite location is considered (as depicted in Figure 2.10), and the differential slant range among those two UEs is computed. From [7]:

$$\Delta D = D_{max}(\alpha_{min}) - D_{min}(\alpha_{max}) \quad (2.5)$$

$$\begin{aligned} \Delta D = & (\sqrt{R_E^2 \sin(\alpha_{min})^2 + h_s^2 + 2R_E h_s - R_E \sin(\alpha_{min})}) - \\ & - (\sqrt{R_E^2 \sin(\alpha_{max})^2 + h_s^2 + 2R_E h_s - R_E \sin(\alpha_{max})}) \end{aligned} \quad (2.6)$$

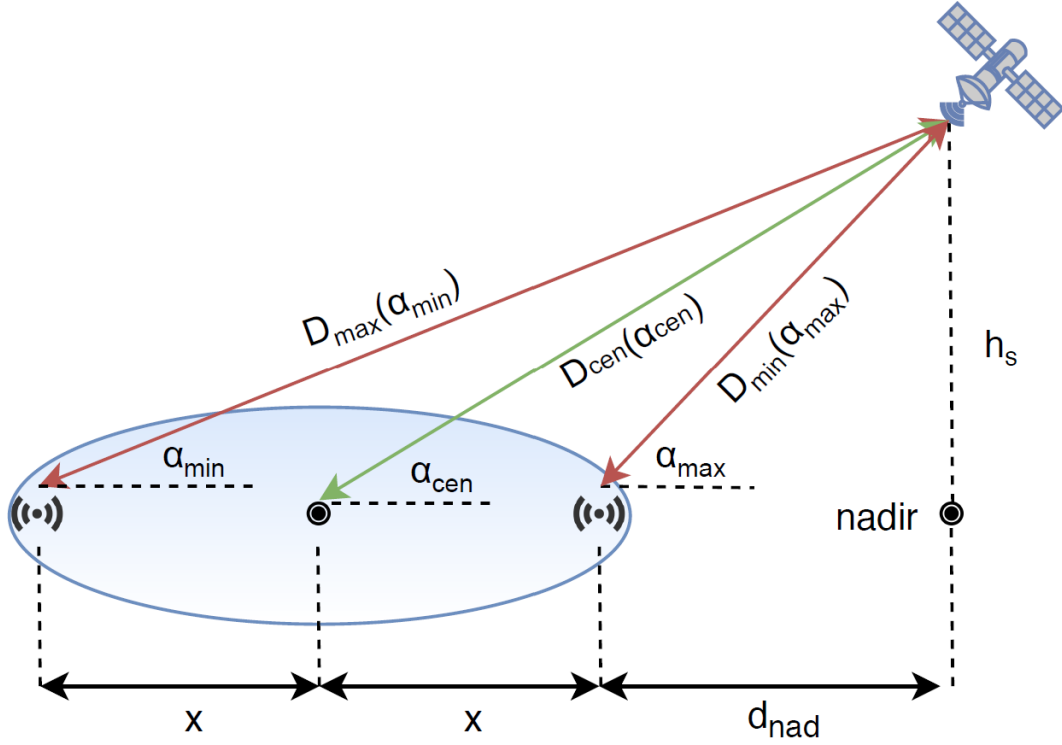


Figure 2.10: System geometry for DPD computation, [7].

Then, the maximum DPD for the considered cell is computed as $\Delta T_{pd} = \frac{\Delta D}{c}$.

2.8 Delay Implications on NB-IoT Procedures

In this Section, the implications of delay on the NB-IoT procedures is analyzed. In Sections 2.8.1 and 2.8.2 the focus is on the possible issues caused by the large RTT on RA and HARQ procedures. Afterwards, in Sections 2.8.3 and 2.8.4 the implications of the DPD on TA and RA procedures are presented.

2.8.1 Large RTT Implications on RA Procedures

When the UEs send the preamble in Message 1 to starting the RA procedure, they wait for a limited time (RAR time window) to receive back the RAR message from the serving eNB. The choice of the RAR time window is performed by the UE depending on the SNR estimation on the downlink signal, and on the number of repetitions used to transmit the NPRACH preamble. It is worth noting that the

chosen RAR time window should be longer than the RTT. In fact, the preamble needs to be transmitted, processed at the eNB, and sent back to the UE before the RAR timer expires.

In LTE the possible RAR time windows are short because it has been designed for short terrestrial RTT ($< 1ms$). On the other hand, in NB-IoT the maximum duration of the RAR time window has been extended up to 10.24 s, [34]. In addition, also the MAC contention resolution timer duration, that can also cause problems in SatCom context, is extended up to 10.24 s, [28]. In summary, the extension of RAR time windows, between message 1 and 2, and of the contention resolution timer, between message 3 and 4 up to 10.24 s, allow to cope with the characteristic RTT of a SatCom system and, thus, no procedure modifications are needed.

2.8.2 Large RTT Implications on HARQ Procedures

The high RTT of SatCom has no implications on the HARQ procedures feasibility in general. Either in the case of data exchange HARQ or Random Access HARQ. Nevertheless, while in the former the RTT arises a problem of increased power consumption, in the latter it can have implications also on the capacity of the cell. In fact, in RA procedure are used two HARQ procedures (in message 3 and in message 4) so the overall procedure time is significantly increased in SatCom implying a degradation of the RA success probability, [7].

2.8.3 DPD Implications on TA Procedure

As discussed in the previous Chapter about NB-IoT, the TA computation is performed from the UE assisted by the eNB and follow the same steps as legacy LTE. The eNB measures the ToA of the RA preamble and sends this information back to the UE with the timing advance command. Upon reception of the command, the UE shall adjust the uplink transmission timing for NPUSCH accordingly to it. In [8] is illustrated that for NB-IoT it is possible to compensate a DPD in the uplink transmission, up to a maximum of 0.6667 ms, which is the same value supported for maximum TA in legacy LTE. This means that, if the DPD of the worst case scenario is lower than 0.6667 ms, no modifications to the TA procedure are needed.

In Figure 2.11 are depicted the results of the simulation performed in [8] using the parameters of Table 2.2. Each line in the graph is associated to a scenario with different cell diameter and orbit altitude, and the zero in the time axis corresponds to the maximum elevation angle of 90° . It can be seen that for each scenario there

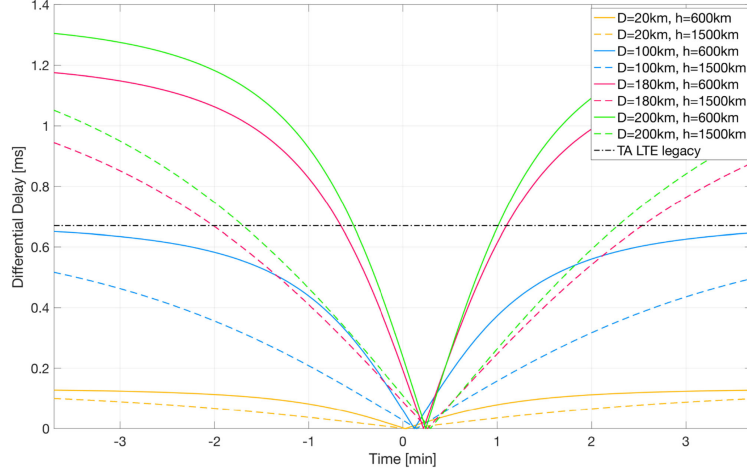


Figure 2.11: Timing Advance analysis, [8].

is a time window for which the maximum DPD is lower than the maximum TA allowed by the protocol. Thus, no modifications to the standard are required if the transmission is performed inside these time windows.

It is worth highlighting that the grater is the cell diameter, the shorter is the allowed transmission time period, keeping the orbit altitude as a constant. Although this do not prevent the protocol to work, it actually imposes a limitation to the maximum cell dimension.

2.8.4 DPD Implications on RA Procedures

Before initiating the RA procedure, the UEs are not yet synchronized in time, since TA procedure is performed later. Therefore, due to differential delay, when many UEs attempt to connect with the eNB through message 1 transmission, their preambles will be misaligned in time. Furthermore, the protocol can work only if the time misalignment does not exceed the preamble CP length.

The requirement on the maximum preamble misalignment can be formalized as:

$$\Delta D < c \cdot T_{cp}/2 \quad (2.7)$$

It is known from (2.5) that ΔD depends on the slant range of the closest and the farthest UEs to the satellite. D_{max} is associated with the elevation angle α_{min} that is set to 10° for this computation. On the other hand, D_{min} is associated with the elevation angle α_{max} that must be evaluated. In fact, α_{max} is the elevation angle

associated to the minimum slant range that ensures the equation (2.7).

After having obtained D_{min} from α_{max} we can calculate the radius of the cell by the low of cosines in a triangle:

$$x = \frac{\sqrt{D_{max}^2 + D_{min}^2 + 2D_{max}D_{min}\cos(\alpha_{max} + \alpha_{min})}}{2} \quad (2.8)$$

In Figure 2.12 is plotted the cell radius as a function of the cell center elevation angle α_{cen} , for the three existing NPRACH configurations. In the graph are emphasized the points where the α_{max} reaches 90 degrees, hence the minimum slant range will coincide with the satellite altitude $D_{min} = h_s$. It is worth noticing that the computations are referred to an orbit altitude of 600 Km, but since DPD decreases with the orbit altitude, the higher the orbit the larger the cell radius would be.

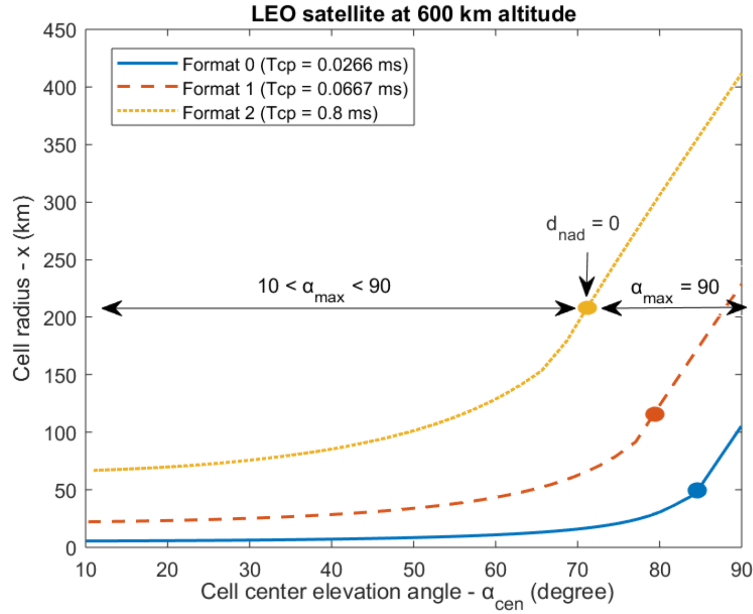


Figure 2.12: Cell radius vs Cell center elevation angle, [7].

2.9 DPD Mitigation Techniques

The analysis presented in the last Section has highlighted the issues caused by DPD on RA and TA procedures. Therefore, in this Section, two DPD mitigation tech-

niques are presented.

2.9.1 Position Tracking

As discussed in Section 2.5.3 for Doppler mitigation, a UE may use its geographical location in combination with satellite ephemeris data to estimate the service link propagation delay. Thus, the transmission of the random access preamble can be time synchronized by compensating for the estimated delay.

Typically, the RA preamble reception is a sensitive operation because the preamble is transmitted by the UEs without any knowledge of their specific propagation delay. Only after the transmission of the TA command the UE can have a more precise time synchronization. By contrast, making use of the GNSS location the UE can be time synchronized already from the first transmission.

2.9.2 New NPRACH Configurations

GNSS is not always a viable solution due to its high power consumption. In this case the only way to increase the cells dimension, as discussed in [7] is to introduce new preambles with longer CP lengths. This can give more degrees of freedom to the eNB in selecting the size of the cell, adapting it to the specific Earth region requirements.

NB-IoT rely on the estimate of the received power to select the appropriate NPRACH configuration. However, to fully exploit this additional NPRACH configurations, the eNB should be able to notify the UE with the information based on its orbit. In fact, this would greatly help the UEs to take proper decisions regarding the NPRACH configuration.

As proposed in [7], the orbit information fields may be included in the DCI along with other fields to continuously update the UEs with new TA values. Since the continuous TA estimation must be done at the eNB using the ToA of signals coming from different UEs, it can not be very precise. Nevertheless, in this way the UEs will be able to remain time-synchronized and avoid multiple RA procedures.

Chapter 3

Downlink Synchronization Implementation

In this Chapter, the implementation of the downlink synchronization simulator is addressed. At first, the algorithm used for NPSS and NSSS detection is presented. Precisely, in Section 3.1 is described the procedure used to estimate the time delay and the CFO from the NPSS, whereas in Section 3.2 is described the procedure used to detect the PCID from the NSSS. Afterwards, the complexity of the algorithm is evaluated. Indeed, the number of operations needed to perform the procedures is computed and the required UE computational power is evaluated. In order to assess the performance of the presented synchronization algorithm, a Monte Carlo simulation is performed. Thus, the structure of the simulator is addressed and the performance outcome is presented.

3.1 NPSS Detection Algorithm

NB-IoT NPSS is dedicated for the selection of the best cell and for synchronization both in time and frequency domain. At start-up, the UE is not synchronized in time with the eNB, thus it does not know on which carrier and at which time it will receive the NPSS from the eNB. Consequently, the UE needs to scan the frequency raster looking for the NPSS. Furthermore, the UE must be able to detect the NPSS without knowing when the NPSS will arrive. NPSS can be detected even in the presence of high CFO, so in this step of the synchronization, the CFO can be neglected. When the UE detects the NPSS on a specific carrier of the frequency raster, it means that it has detected the presence of a eNB anchor carrier and the synchronization

procedure can continue. Now the UE has synchronized with the frame timing of the UE but must synchronize also in frequency. Indeed, the presence of the CFO can prevent the transmission to work properly, and must be compensated.

In this Section, the synchronization algorithm developed to recover the time frame alignment and the CFO is described.

In order to derive the synchronization signal received by the UE, the NPSS is firstly defined. The NPSS is generated relying on Zadoff-Chu sequences. According to [14], the l -th NPSS symbol, with $l = 3, 4, \dots, 13$, at the n -th subcarrier, with $n = 0, 1, \dots, 10$, can be expressed as:

$$d_l(n) = s(l) \cdot \exp\left(-j \frac{5\pi n(n+1)}{11}\right) \quad (3.1)$$

where $s(l) = [1, 1, 1, 1, -1, -1, 1, 1, 1, -1, 1]$. Then, the transmitted signal $x(t)$ is generated by mapping $d_l(n)$ on the radio elements and performing an OFDM modulation. At the receiver side, after the demodulation, the equivalent baseband signal is given by:

$$r(t) = x(t-s) \cdot h e^{j2\pi CFO(t-s)} + n(t) \quad (3.2)$$

where h refers to the channel impulse response, s denotes the time delay and $n(t)$ is the Additive White Gaussian Noise (AWGN) filtered on the receiver bandwidth.

Afterwards, the received signal $r(t)$ is sampled with a sampling rate of 1.92 MHz leading to the sampled received signal $r(n)$. The NPSS has a time periodicity of one frame, thus, though there is still no information about the frame timing, it is possible to perform a coherent accumulation of the frame samples. In fact, the frame length expressed in samples is $N_\omega = 10ms \cdot 1.92MHz = 19200$, so the samples $r(k)$ and $r(2N_\omega + k)$ belongs to the first and the second frame but share the same frame timing. Thus, averaging the samples which share the same frame timing, over the N consecutively received frames, a coherent combining of the samples is obtained. Since NPSS repeats itself in every frame, making use of this accumulation it is possible to improve the detection. It can be formalized as:

$$\bar{r}_m(n) = \frac{1}{N} \sum_{k=0}^{N-1} r(kN_\omega + n) \quad n = 1, 2, \dots, N_\omega \quad (3.3)$$

In order to synchronize in time with the received signal, the time position of the known NPSS signal must be detected in the samples $\bar{r}_m(n)$. Specifically, a maximum correlation algorithm is applied to the received signal, in order to find the time delay hypothesis \bar{s} which leads to maximum correlation with the reference NPSS sequence $P(n)$. $P(n)$ is the sampled version of $d_l(n)$ in time domain, and its length is $N_r = ((128 + 9) \cdot 11) + 1 = 1508$ samples, with the one additional sample being the extra IFFT point at the 7th OFDM symbol.

As a first step, the cross-correlation between $\bar{r}_m(n)$ and the reference NPSS sequence $P(n)$ on a one frame window is performed in (3.4).

$$\Lambda(\bar{s}) = \sum_{n=\bar{s}}^{\bar{s}+N_r-1} |P(n - \bar{s}) \cdot \bar{r}_m^*(n)| \quad (3.4)$$

Thus, the time frame alignment \hat{s} is determined by the time delay hypothesis \bar{s} which maximizes the cost function $\Lambda(\bar{s})$:

$$\hat{s} = \arg \max_{\bar{s} \in [0, N_\omega]} \Lambda(\bar{s}) \quad (3.5)$$

At start-up, to find a cell to camp on, the UE keeps searching for a peak in the cost function (3.4) in all the possible eNB frequencies. When it finds the peak, it means it has detected a NPSS with its time offset \hat{s} , and it can continue with the following synchronization steps.

In this work the CFO is recovered by estimating the frequency offset between the CPs of the time synchronized signal. A NB-IoT OFDM symbol is composed by a CP followed by the data signal. Thus the total number of samples in a OFDM symbol is $S_O = CP_{length} + nFFT$, where CP_{length} and $nFFT$ are the number of samples of the CP and of the data signal, respectively. The presence of the CFO introduces a frequency shift at every sampling instant, which is proportional to the CFO normalized to the sampling frequency. Indeed, the phase shift θ_n , introduced

by the CFO, between the sample in position m and the sample in position $m + n$ of a OFDM symbol is:

$$\theta_n = 2\pi \cdot CFO \cdot (nT_{samp}) \quad (3.6)$$

where T_{samp} is the sampling time interval. Now we define header (h) and tail (t) as in Figure 3.1. h is constituted by the samples of the CP, thus the first CP_{length} samples of the OFDM symbol; and t is constituted by the last CP_{length} samples of the OFDM symbol.

$$\begin{aligned} h_m &= r_{ofdm}(n) & n &= 1, \dots, CP_{length} \\ t_m &= r_{ofdm}(n) & n &= 1 + nFFT, \dots, S_O \end{aligned} \quad (3.7)$$

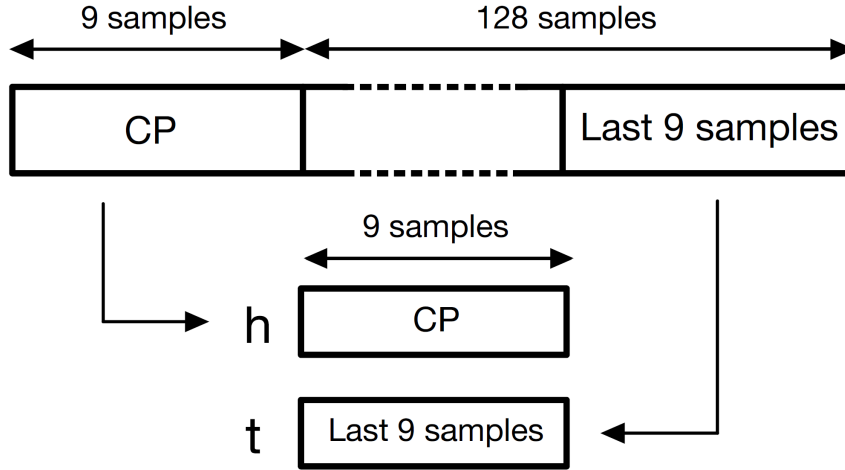


Figure 3.1: h and t extraction in one OFDM symbol.

where h_m and t_m are the samples in position m of h and t respectively, and $r_{ofdm}(n)$ is the n -th sample of a considered OFDM symbol. Since the CP is nothing more than the last CP_{length} samples of the OFDM symbol repeated in the head of the symbol, h_m and t_m contains the same information, thus they have the same amplitude and phase related to the information. However, they differ of a frequency

offset $\theta = 2\pi \cdot CFO \cdot (nFFT \cdot T_{samp})$, due to the CFO and to their time separation in the OFDM symbol. It is formalized as:

$$t_m = h_m \cdot e^{j2\pi \cdot CFO \cdot (nFFT \cdot T_{samp})} \quad (3.8)$$

being $nFFT$ the number of samples between h_m and t_m . As a consequence, in order to extract the frequency shift introduced by $nFFT$ samples, is possible to perform a multiplication between the h samples and the complex conjugate of t . In fact, it is computed as:

$$C_m = h_m \cdot t_m^* = h_m \cdot h_m^* e^{-j\theta} = |h_m|^2 e^{-j\theta} \quad (3.9)$$

The result of the multiplication is the squared module of the sample, thus the phase associated to the information and to the common CFO phase is lost and only the phase difference θ induced by the CFO remains. Since $\theta = 2\pi \cdot CFO \cdot (nFFT \cdot T_{samp})$, the CFO can be easily computed from the argument of C_n divided by $2\pi \cdot nFFT \cdot T_{samp}$.

$$C\hat{F}O = \frac{\angle C_m}{2\pi \cdot nFFT \cdot T_{samp}} \quad (3.10)$$

This CFO estimation is presented considering only one couple of sample (h_m, t_m) for the sake of simplicity. However, it is obviously necessary to repeat it for all the received CP samples in order to obtain a reliable estimation of the CFO, thus, a sequence of N_{sf} subframes r_{sf} is taken as a reference. The conjugate multiply of the headers with the tails is performed multiplying r_{sf} by the conjugate of itself shifted by $nFFT$ samples. In fact, $nFFT$ is the distance between h and t in a given OFDM symbol, thus, after the circular shifting of r_{sf} by $nFFT$ samples, the tails will be superimposed to the headers of the original sequence. The shifted sequence T and the original sequence H are defined as in (3.11) and their conjugate multiply is expressed in (3.12).

$$H(m) = r_{sf}(n) \quad n = 1, \dots, end - nFFT \quad (3.11)$$

$$\begin{aligned}
T(m) &= r_{sf}(n) \quad n = 1 + nFFT, \dots, end \\
C &= H \cdot T^*
\end{aligned} \tag{3.12}$$

Afterwards, computing the mean over all the CP samples present in C is possible to average out the phase noise and obtain a more precise estimation. Calling \overline{C} the averaged C , $C\hat{FO}$ is obtained by:

$$C\hat{FO} = \frac{\angle \overline{C}}{2\pi \cdot nFFT \cdot T_{samp}} \tag{3.13}$$

3.2 NSSS Detection Algorithm

NSSS detection procedure is fundamental in order to identify the eNB by means of its PCID, and to synchronize with the 80 ms NSSS repetition time window. Indeed, the eNB embeds its PCID in the NSSS sequence, thus detecting the NSSS means to detect the eNB PCID.

In this Section the detection algorithm developed to detect the PCID embedded in the NSSS is described.

The NSSS sequence is formulated by multiplying a ZC sequence and a binary complementary sequence such that:

$$K_m^{PCID}(g) = m_n(g') e^{-j2\pi u g} e^{-j\pi PCID' g''(g''+1)/(M-1)}, \quad 0 \leq g < M \tag{3.14}$$

where $M = 132$ is the length of NSSS sequence, $n = \text{int}(v/126)$, PCID belongs to $[0, 1, 2, \dots, 503]$, $g' = (g \bmod 128)$, $g'' = (g \bmod 131)$, $PCID' = (PCID \bmod 126) + 3$, $u = (n_f/8 \bmod 4)$ is associated with the Radio Frame Number (RFN) n_f , and $m_n(g')$ is one of the four length- M complementary sequences.

Initial time and frequency synchronization is accomplished exploiting NPSS on the modulated received signal $r(t)$. On the contrary, the NSSS detection is performed on the OFDM demodulated signal $R_{l,p}(n)$, where the notation indicates the l OFDM symbol on the p subcarrier, on the n -th subframe. Thus, as a first step the OFDM symbols are generated from the Fast Fourier Transform (FFT) unit and then the UE attempts to acquire the PCID by detecting the NSSS in this time-frequency domain. The optimal NSSS detection performances are attained with the exhaustive Maximum Likelihood (ML) search-based method. It compares all the potential combinations of ZCs and complementary sequences with the received NSSS sequence, obtaining a computationally demanding but detection-optimal algorithm.

The received signal $R_{l,p}(n)$ is considered in a window of N_f frames. In addition, all the subframes of $R_{l,p}(n)$ associated with NSSS are called $R_{l,p}^{SSS}(n)$, as depicted in Fig 3.2. The first step of the algorithm is to cross correlate $R_{l,p}^{SSS}(n)$ with the known NSSS sequence K_m^{PCID} , where the notation indicates the NSSS associated to a specific PCID with complementary sequence m . The resultant correlation for the specific PCID on the NSSS subframe n is:

$$C_{l,p}^{PCID}(n, m) = R_{l,p}^{SSS}(n) \cdot K_m^{*PCID} \quad (3.15)$$

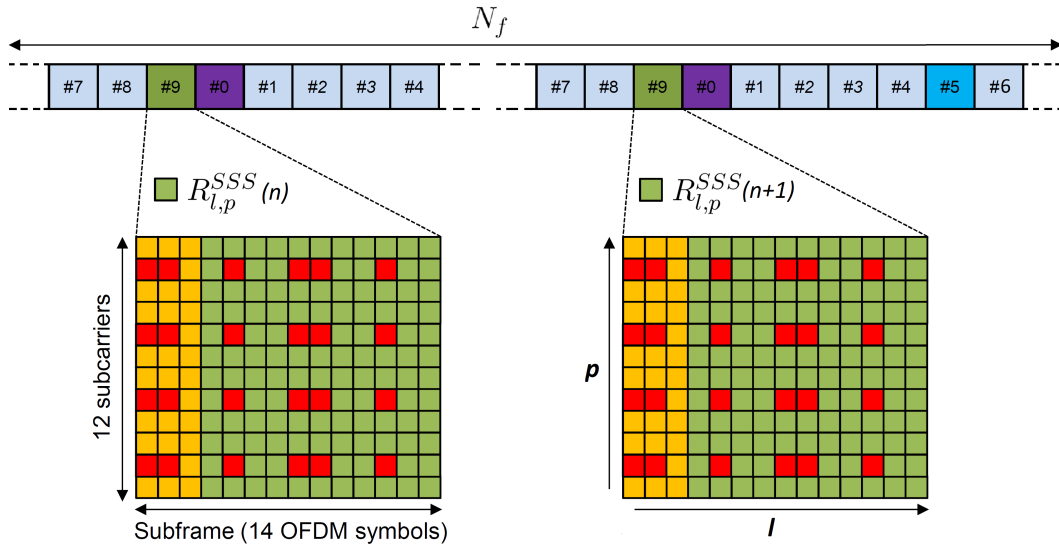


Figure 3.2: Representation of the considered N_f frames.

Afterwards, a coherent accumulation is performed for all NSSS subframes taking the mean on the N_{os} OFDM Symbols and N_{sc} subcarriers. This procedure allows to decrease the power of the noise, thus it increases the correlation SNR.

$$\bar{C}^{PCID}(n, m) = \frac{1}{N_{os} \cdot N_{sc}} \sum_{p=0}^{N_{sc}} \sum_{l=0}^{N_{os}} C_{l,p}^{PCID}(n, m) \quad (3.16)$$

Finally, the non-coherent accumulation across all NSSS subframes is performed taking the mean of $|\bar{C}^{PCID}(n, m)|^2$ on the N_{os} subframes and selecting the maximum between the m results. In fact, the NSSS related to a specific PCID has $m = 4$ different declinations depending on the complementary sequence. Thus all the four hypotheses are evaluated and only the one that leads to maximum correlation is selected. More precisely:

$$C_{tot}^{PCID} = \max_{m \in [1,4]} \sqrt{\frac{1}{N_f} \sum_{n=1}^{N_f} |\overline{C}^{PCID}(n, m)|^2} \quad (3.17)$$

Finally, the computation of C_{tot}^{PCID} must be performed for all the 502 PCIDs, then the detected PCID is the one that leads to maximum C_{tot}^{PCID} .

$$PCID = \arg \max_{PCID \in [1,502]} C_{tot}^{PCID} \quad (3.18)$$

3.3 Complexity Evaluation

In this Section, the computational burden of the presented algorithm is computed with respect to Floating Point Operations (FPO). The algorithm complexity evaluation is of utmost importance since the NB-IoT UE generally has low computational power. Furthermore, the downlink synchronization is one of the most computationally heavy procedures. Thus synchronization procedure complexity has to be taken into account when computing the minimum required computational power of the UE. As assumed in [35], one complex multiplication, one complex addition, and one complex magnitude are considered equivalent to six, two, and three FPO, respectively. Furthermore, it is assumed that the known NPSS sequence $P(n)$ and NSSS sequences K_m^{PCID} are available at the receiver a priori.

3.3.1 Complexity Of Time Delay Estimation

Every computation of equation (3.4) requires N_r complex multiplications, thus its computation for every possible delay $\bar{\tau}$ requires a total of $N_r \cdot (N_\omega + N_r)$ complex multiplications. In equation (3.5) is searched the maximum between all the correlation results, thus $N_\omega + N_r$ complex magnitude and $N_\omega + N_r$ additions are required.

To summarize, a total of $N_r \cdot (N_\omega + N_r)$ complex multiplications, $N_\omega + N_r$ complex magnitude and $N_\omega + N_r$ additions. These correspond to $(6N_r + 5)(N_\omega + N_r)$ FPO.

3.3.2 Complexity Of CFO Estimation

The computation of C in equation (3.12) requires $(N_{os} \cdot S_O \cdot N_{sf}) - nFFT$ complex multiplications. Then it is needed to take the mean over all the $N_{os} \cdot CP_{length} \cdot N_{sf}$ CP samples in C , and it requires $N_{os} \cdot CP_{length} \cdot N_{sf}$ complex sums. The final step in

equation (3.13) requires 35 multiplications and 5 sums to compute $\arg \bar{C}$ exploiting a Taylor series plus one division.

In summary, a total of $(N_{os} \cdot S_O \cdot N_{sf}) - nFFT + 35$ complex multiplications and $(N_{os} \cdot CP_{length} \cdot N_{sf}) + 5$ complex sums. These correspond to $N_{sf} \cdot (6N_{os}S_O + 2N_{os}CP_{length}) + 220 - 6nFFT$ FPO.

3.3.3 Complexity Of PCID detection

The correlation Performed in equation (3.15) requires $4 \cdot N_{sc} \cdot N_{os} \cdot N_f$ complex multiplications. The succeeding coherent combining in (3.15) requires $4 \cdot N_{sc} \cdot N_{os} \cdot N_f$ complex sums. Afterwards, to perform the non-coherent combining and to determine the PCID-specific correlation C_{tot}^{PCID} are required N_f complex magnitudes, $2N_f + 10$ multiplications and $N_f + 10$ sums. In this last computation the square root is computed with the Newton method.

Finally, the computation of C_{tot}^{PCID} must be performed for all the possible PCIDs. Thus, the operation described so far must be repeated N_{PCID} times. Then, to find the PCID that maximizes C_{tot}^{PCID} are required N_{PCID} additional sums.

To summarize, a total of $N_{PCID} \cdot [(4 \cdot N_{sc} \cdot N_{os} \cdot N_f) + 2N_f + 10]$ complex multiplications, $N_{PCID} \cdot [(4 \cdot N_{sc} \cdot N_{os} \cdot N_f) + 2N_f + 10] + N_{PCID}$ complex sums and N_f complex magnitudes. These correspond to $8N_{PCID} \cdot [(4 \cdot N_{sc} \cdot N_{os} \cdot N_f) + 2N_f + 10] + 2N_{PCID} + 3N_f$ FPO.

3.3.4 Required UE computational power

In this Section is computed the number of FPO needed to carry out the time delay estimation, CFO estimation and PCID detection, taking as a reference the values of Table 3.1.

Regarding NPSS detection and time delay estimation, the number of FPO is computed as $(6N_r + 5)(N_\omega + N_r)$ and results to be $1.87 \cdot 10^8$ FPO.

For what concerns the CFO estimation, the number of operations depends on the number of subframes N_{sf} considered in the algorithm. In the presented implementation, a time window of one frame is selected, so $N_{sf} = 10$. As a consequence, the number of FPO is computed as $N_{sf} \cdot (6N_{os}S_O + 2N_{os}CP_{length}) + 220 - 6nFFT$ and results to be $1.17 \cdot 10^5$ FPO.

Finally, in the presented implementation the PCID detection is performed over a time window of four frames so $N_f = 4$. Consequently, the number of FPO is

computed as $8N_{PCID} \cdot [(4 \cdot N_{sc} \cdot N_{os} \cdot N_f) + 2N_f + 10] + 2N_{PCID} + 3N_f$ and results to be $1.08 \cdot 10^7$ FPO.

To assess the required UE computational power, must be taken in to account also the time window in which this FPO are computed. Both time delay and CFO are estimated over a time window of one frame, while the detection of PCID has more relaxed time requirements. Thus, it appears clear that the most computational power demanding is the NPSS detection and time delay estimation part. Indeed, it requires $1.87 \cdot 10^8$ FPO multiplied by $10ms$ frame duration, resulting in a total of $1.87 \cdot 10^{11}$ FPO Per Second (flops). On the other hand, CFO estimation and PCID detection requires only $1.17 \cdot 10^7$ flops and $4.32 \cdot 10^5$ flops respectively.

<i>Abbreviation</i>	<i>Meaning</i>	<i>Typical value</i>
N_r	Length of known NPSS sequence $P(n)$	1508
N_ω	Number of samples in one frame	19200
S_O	Number of samples in one OFDM symbol	137
N_{os}	Number of OFDM symbols in one subframe	14
N_{sc}	Number of downlink subcarriers	12
$nFFT$	Dimension of the FFT	128
CP_{length}	Number of samples in one CP	9 or 10
N_{PCID}	Number of possible PCIDs	502
N_{sf}	Subframes considered for CFO estimation	10
N_f	Frames considered for PCID detection	4

Table 3.1: Values considered for computational power assessment.

3.4 Performances

In order to evaluate the performances of the illustrated synchronization algorithm, the NB-IoT downlink synchronization block has been simulated in MATLAB assuming: i) 15 kHz sub-carrier spacing, ii) a sampling rate of 1.92 MHz, iii) 128-point FFT and a single antenna at receiver, iv) AWGN standard channel was considered. Simulations were performed over 10^6 frames over independent channel realizations.

To assess the performances two metrics has been defined. The error probability for the time delay estimation ($P_e^{delay} = Errors/N_D$), and the error probability the PCID detection after a correct time delay estimation ($P_e^{PCID}|_{Sync}$). The analysis of the two performance metrics is performed by means of Monte Carlo simulations.

As a first step, the simulator must generate the downlink signal on which the algorithm is performed. Thus, it generates an array of samples $r(n)$ of the downlink signal, which corresponds to a specific PCID, in a time window of four frames. Afterwards, it introduces the time delay s by means of a shifting of the array of s positions, obtaining $r^d(n)$. The AWGN channel is considered by adding the noise samples $n_{SNR}^N(n)$ to $r^d(n)$, where the notation indicates the noise associated to a specific Signal to Noise Ratio (SNR) power and N-th iteration of the Monte Carlo simulation.

The Monte Carlo simulation to measure P_e^{delay} and $P_e^{PCID}|_{Sync}$ consists in N_D iterations of the algorithm, in which the noise samples $n_{SNR}^N(n)$ are independent among the iterations. Specifically, in every iteration N the noisy received signal $r_{AWGN}^d(n) = r^d(n) + n_{SNR}^N(n)$ is elaborated by the synchronization algorithm in order to extract \hat{s} and $C\hat{F}O$. Then P_e^{delay} and $P_e^{PCID}|_{Sync}$, for the specific SNR value, are computed by counting the number of errors and dividing it by N_D .

3.4.1 Time Delay Probability Of Error

At first, a simulation without accumulation is performed and the NPSS is searched in a single frame. However, since for the NPSS detection is possible to accumulate the samples received in different frames as expressed in equation (3.3), a second simulation with accumulation of four frames is performed. The former is shown in Figure 3.3, while the latter is shown in Figure 3.4. The first part of the simulation, in which the downlink signal is generated and delayed of s samples, is common to all the iteration. In contrast, at each iteration different noise samples must be considered, thus, the noise generation and its addition to the signal, is performed inside the cycle. At every iteration N , the simulator follows the steps described in section 3.1 in order to estimate \hat{s} . Finally, P_e^{delay} is derived from the number of iteration that have lead to an estimation error ($\hat{s} \neq s$).

Considering the simulation without frame accumulation, the value of P_e^{delay} is simulated for SNRs equal to -14, -12, -10, -9, -8, -6, -4, -2 and 0 dB, obtaining the results shown in Figure 3.6. Additionally, the results for the simulation using frame accumulation, for the same SNR values, are depicted in Figure 3.7. It is worth

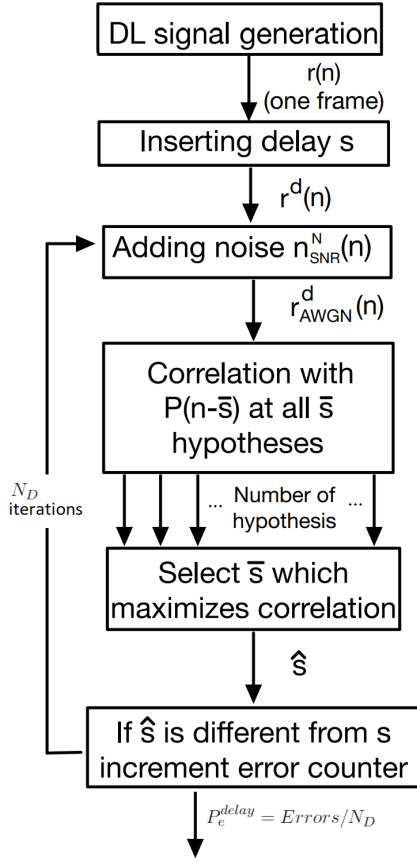


Figure 3.3: NPSS detection simulator scheme without accumulation.

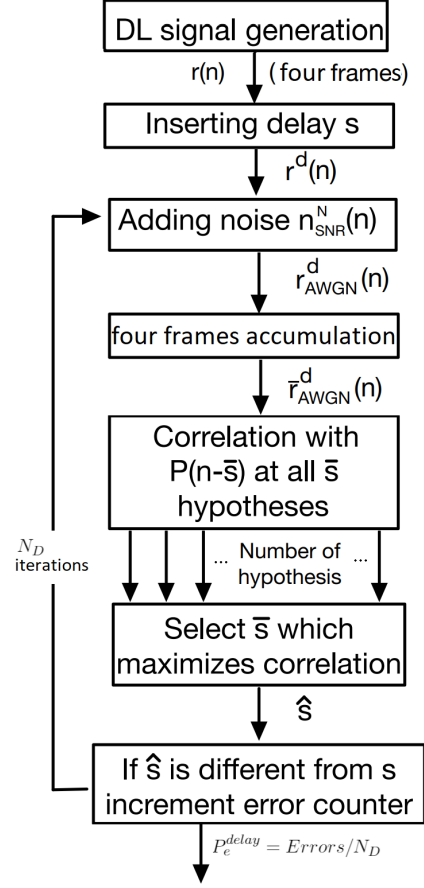


Figure 3.4: NPSS detection simulator scheme with accumulation of four frames.

noticing that the accumulation technique has produced a considerable performance, however, it implies an higher estimation latency, proportional to the number of accumulated frames.

The coherent combining of the frame samples produces a computational gain that is equal to the number of accumulated frames N_f^{acc} . In fact, the noise in input is a random normally distributed variable with mean equal to 0 and variance σ^2 and, after the coherent summation, the probability distribution is still normal, but its variance is divided by the number of coherent accumulations N_f^{acc} , [36]. Thus, the SNR is increased by $10 \log_{10}(N_f^{\text{acc}})$ dB. In the considered implementation $N_f^{\text{acc}} = 4$ so the gain is $10 \log_{10}(4) = 6$ dB. This result is found also in the simulations outcomes, in fact, from Figure 3.8 is clear that the P_e graph with accumulation is translated to the left of 6 dB respect to the graph without accumulations.

3.4.2 PCID Detection Probability Of Error

The NSSS detection is heavily affected by CFO and timing delay. Indeed, since NSSS sequence spreads across multiple OFDM symbols, the presence of CFO would introduce high distortion into the received sequence. For example, even a small CFO may introduce a phase difference up to 2π across the whole NSSS sequence[18], implying that half of the sequence suffers from sign negation. Thus, since the sign may be the only differentiation between two NSSS sequences a possible consequence is to incorrectly detect the desired sequence. Furthermore, for large time delays a similar impact can be noticed. For these reasons PCID detection performances are affected by the accuracy of the time delay and CFO estimation performed in the first step.

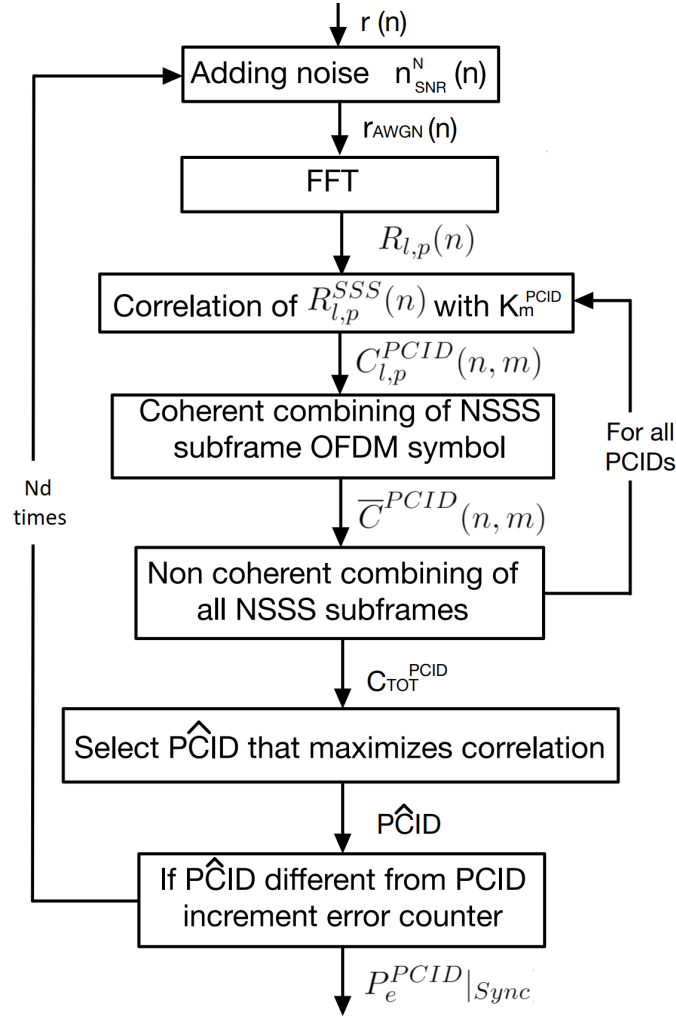


Figure 3.5: NPSS detection simulator scheme without accumulation.

In this second step of the simulation the interest is the PCID detection only. Thus, to prevent the P_e^{PCID} computation to be conditioned by P_e^{delay} , the simulation is performed assuming an input signal perfectly time and frequency synchronized. The structure of the simulation is shown in Figure 3.5. The perfect time synchronization is simulated simply not introducing the time delay in the input signal. Furthermore, a different noise realization is considered inside each iteration in order to have a statistical independent result at each cycle. Then, for all possible PCIDs, the correlation of the known NSSS and the received signal is computed and the PCID that yields to maximum correlation is selected. Finally P_e^{PCID} is derived from the number of iteration that have lead to an estimation error ($PCID \neq \hat{PCID}$).

The output of the simulation $P_e^{PCID}|_{sync}$ for SNRs from -21 to -6 dB is depicted in Figure 3.9. The lower value of the SNRs range is defined by the gain introduced by the algorithm. In fact, the coherent combining performed in equation (3.16) enhances the signal SNR by a factor of 132, equivalent to 21.2dB. Thus, the input signal cant be lower than $-21.2dB$ to perform the PCID detection. This algorithm gain is due to the averaging of all the 132 correlation values in a NSSS subframe, this implies a summation and the subsequent division by 132. Indeed, following [36], the SNR in input is E_s/N_0 and after this operation E_s remains constant while the noise variance is reduced by a 132 factor. Hence, the SNR is increased by the same quantity.

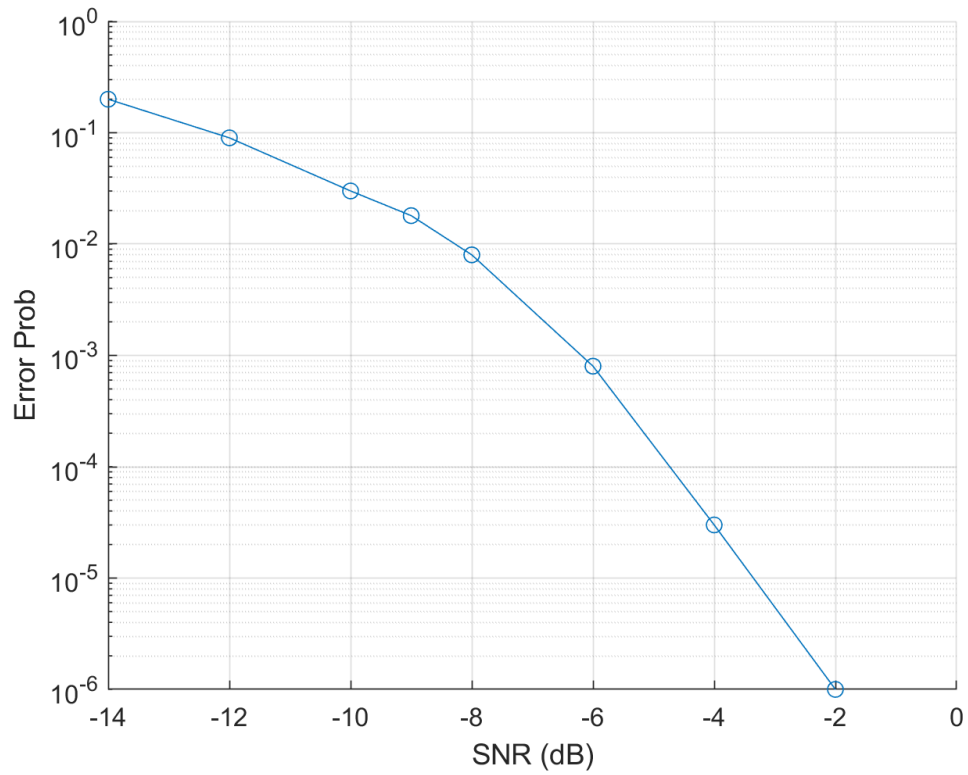


Figure 3.6: Simulation results for P_e^{delay} without accumulation.

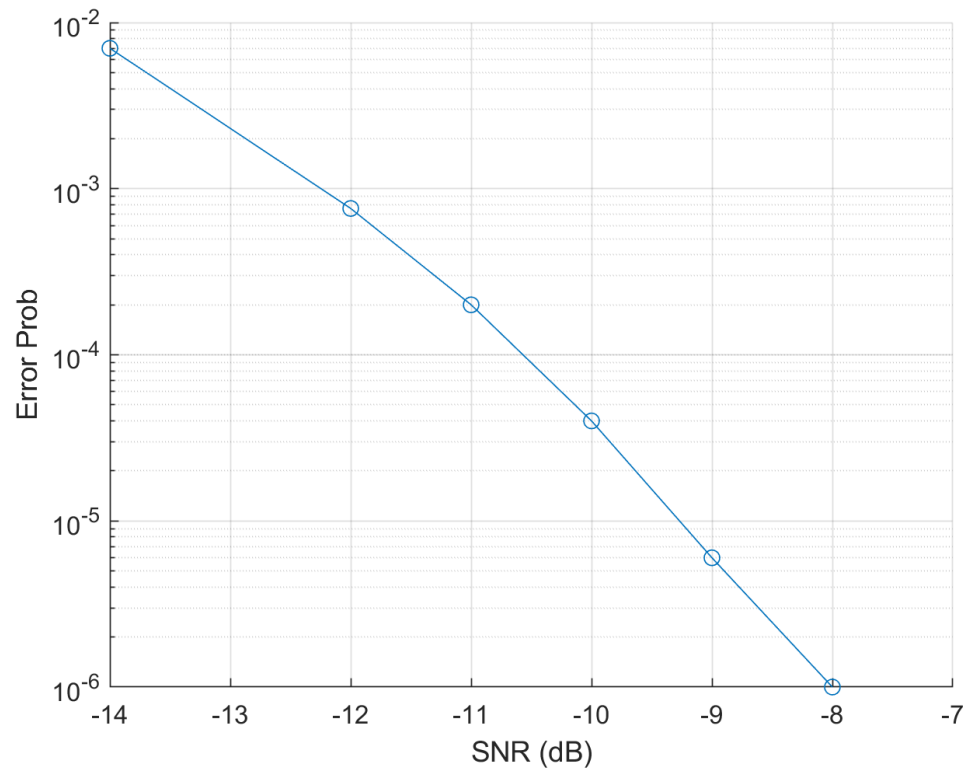


Figure 3.7: Simulation results for P_e^{delay} with accumulation of four frames.

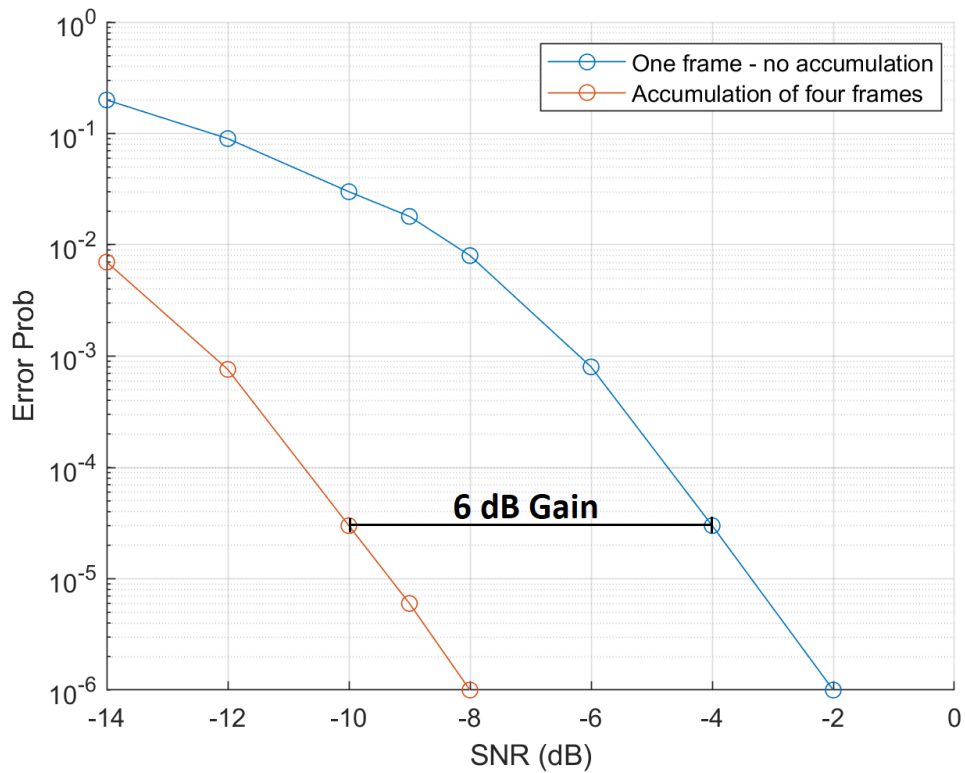


Figure 3.8: Comparison between P_e^{delay} with accumulation and without accumulation.

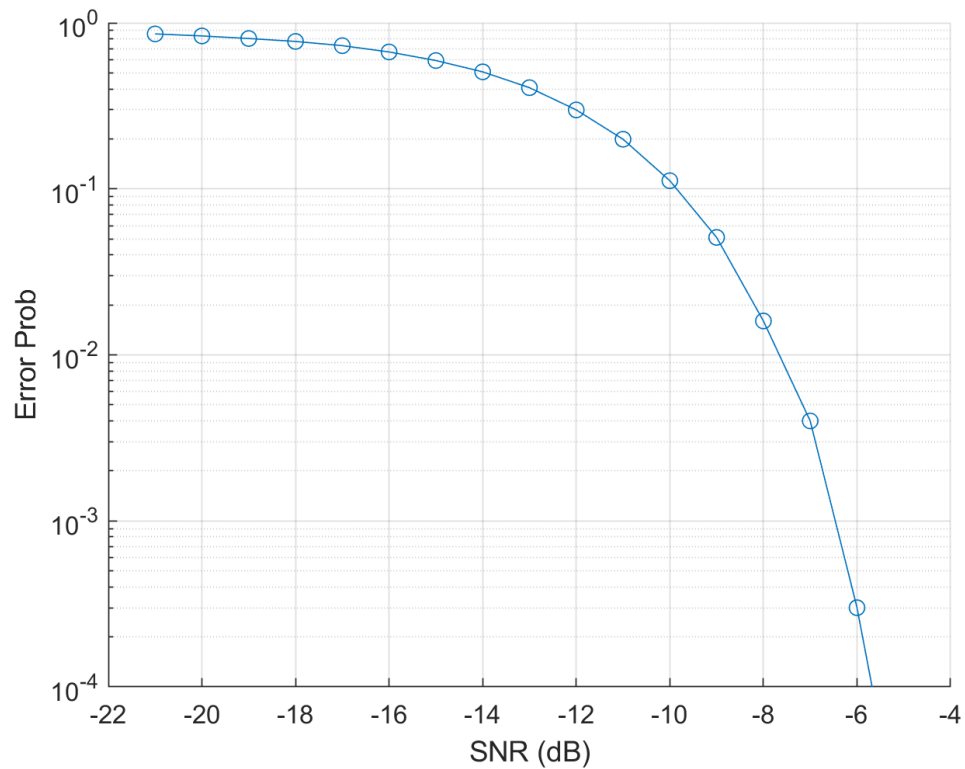


Figure 3.9: Simulation results for $P_e^{PCID}|_{Sync}$ on a window of four frames.

Chapter 4

Conclusions

The main objective of this thesis was to build the simulator of a NB-IoT user equipment. In the NB-IoT protocol, the downlink Synchronization procedure is of fundamental importance, since it is the first procedure that the user equipment must perform at start-up in order to synchronize with the eNB. Hence, as a first step, the work has focused on the downlink synchronization procedure in the SatCom system.

The impact of the satellite channel impairments on the NB-IoT terrestrial technology, was analyzed. At first, the NB-IoT technology was presented, and the protocol procedures were detailed. Then, the analysis of the most important satellite channel impairments was presented. In particular, the impact of the Doppler and propagation delay on the most important NB-IoT procedures was analyzed, with particular attention on the synchronization procedure. At this purpose, the analysis of the SoA techniques counteract these impairments has been reviewed.

By means of MATLAB, a simulator of the downlink synchronization procedure has been analyzed. Finally, the performances of the implemented synchronization algorithm has been measured by means of numerical simulations. In conclusion:

- The Doppler shift introduced by the satellite channel is often larger than maximum Doppler defined in the 3GPP requirements for NB-IoT. The SoA techniques proposed for Doppler mitigation are: i) frequency advance; ii) CP based and MAP based Doppler estimation; iii) position tracking; iv) resource allocation strategy.
- From the literature analysis of delay impact over the NB-IoT protocol, emerged that large RTT can be overcome. However, the analysis has highlighted the need for efficient differential delay compensation techniques, in order to make

NB-IoT compatible with NTN. The SoA techniques proposed for differential delay mitigation are: i) introduction of new NPRACH configurations; ii) position tracking.

- The downlink synchronization algorithm has shown good performances in the AWGN channel. However, an optimization of the algorithm is needed in order meet the computational capabilities of a NB-IoT terminal.

Future works foresee the implementation of a complete simulation of the NB-IoT protocol, thus, all the remaining NB-IoT procedures will be investigated. Additionally, the synchronization algorithm complexity evaluation could be exploited to realize an hardware implementation and/or to perform a porting on different languages.

Bibliography

- [1] Olof Limberg, Marten Sunderberg, Eric Wang, Joahn Bergman, and Joachim Sachs, *Cellular internet of things from massive deployment to critical 5G applications*, Elsevier, 2020.
- [2] Ahmad El Fawal, Ali Mansour, Mohamad Najem, Denis Le Jeune, and Frederic Le Roy, “Ctmc modeling for m2m/h2h coexistence in a nb-iot adaptive enodeb,” 07 2018.
- [3] Rohde & Schwarz, “Application note narrowband internet of things measurements,” .
- [4] R. Ratasuk, J. Tan, Nitin Mangalvedhe, M. H. Ng, and A. Ghosh, “Analysis of nb-iot deployment in lte guard-band,” *2017 IEEE 85th Vehicular Technology Conference (VTC Spring)*, pp. 1–5, 2017.
- [5] Telit, “Psm application note,” .
- [6] Mamta Agiwal, Mukesh Maheshwari, and Hu Jin, “Power efficient random access for massive nb-iot connectivity,” *Sensors*, vol. 19, pp. 4944, 11 2019.
- [7] O. Kodheli, N. Maturo, S. Chatzinotas, S. Andrenacci, and F. Zimmer, “On the random access procedure of nb-iot non-terrestrial networks,” in *2020 10th Advanced Satellite Multimedia Systems Conference and the 16th Signal Processing for Space Communications Workshop (ASMS/SPSC)*, 2020, pp. 1–8.
- [8] A. Guidotti, A. Vanelli-Coralli, M. Conti, S. Andrenacci, S. Chatzinotas, N. Maturo, B. Evans, A. Awoseyila, A. Ugolini, T. Foggi, L. Gaudio, N. Alagha, and S. Cioni, “Architectures and key technical challenges for 5g systems incorporating satellites,” *IEEE Transactions on Vehicular Technology*, vol. 68, no. 3, pp. 2624–2639, 2019.

- [9] M. Conti, S. Andrenacci, N. Maturo, S. Chatzinotas, and A. Vanelli-Coralli, "Doppler impact analysis for nb-iot and satellite systems integration," in *ICC 2020 - 2020 IEEE International Conference on Communications (ICC)*, 2020, pp. 1–7.
- [10] Ericsson, "Ericsson mobility report," [online], 2017, Available:<https://www.ericsson.com/assets/local/mobility-report/documents/2017/ericsson-mobility-report-june-2017.pdf>.
- [11] Borja Martinez, Ferran Adelantado, Andrea Bartoli, and Xavier Vilajosana, "Exploring the performance boundaries of nb-iot," *IEEE Internet of Things Journal*, vol. 6, no. 3, pp. 5702–5712, Jun 2019.
- [12] Hossam Fattah, *5G LTE Narrowband Internet of Things (NB-IoT)*, CRC Press, 2018.
- [13] R. Ratasuk, N. Mangalvedhe, Z. Xiong, M. Robert, and D. Bhatoolaul, "Enhancements of narrowband iot in 3gpp rel-14 and rel-15," in *2017 IEEE Conference on Standards for Communications and Networking (CSCN)*, 2017, pp. 60–65.
- [14] S. Zhang, S. Zeng, F. Ye, R. Tang, P. Wu, and M. Xia, "An efficient down-link receiver design for nb-iot," in *2020 IEEE Wireless Communications and Networking Conference (WCNC)*, 2020, pp. 1–6.
- [15] Y. . E. Wang, X. Lin, A. Adhikary, A. Grovlen, Y. Sui, Y. Blankenship, J. Bergman, and H. S. Razaghi, "A primer on 3gpp narrowband internet of things," *IEEE Communications Magazine*, vol. 55, no. 3, pp. 117–123, 2017.
- [16] Yong Shi, "Power saving methods for lte-m and nb-iot devices white paper," .
- [17] H. Ni, G. Ren, and Y. Chang, "Complexity effective cell search scheme for ofdm cellular system," in *2010 IEEE International Conference on Communication Systems*, 2010, pp. 700–704.
- [18] A. Ali and W. Hamouda, "On the cell search and initial synchronization for nb-iot lte systems," *IEEE Communications Letters*, vol. 21, no. 8, pp. 1843–1846, 2017.

- [19] Young-Hwan You, “Reduced complexity detection of narrowband secondary synchronization signal for nb-iot communication systems,” *Symmetry*, vol. 12, pp. 1342, 08 2020.
- [20] S. Cho, H. Kim, and G. Jo, “Determination of optimum threshold values for nprach preamble detection in nb-iot systems,” pp. 616–618, 2018.
- [21] X. Lin, A. Adhikary, and Y. . Eric Wang, “Random access preamble design and detection for 3gpp narrowband iot systems,” *IEEE Wireless Communications Letters*, vol. 5, no. 6, pp. 640–643, 2016.
- [22] M. De Sanctis, E. Cianca, G. Araniti, I. Bisio, and R. Prasad, “Satellite communications supporting internet of remote things,” *IEEE Internet of Things Journal*, vol. 3, no. 1, pp. 113–123, 2016.
- [23] 3GPP, “Ts 38.811, study on new radio (nr) to support non-terrestrial networks, v15.2.0,” 2019.
- [24] O. Liberg, S. E. Lowenmark, S. Euler, B. Hofstrom, T. Khan, X. Lin, and J. Sedin, “Narrowband internet of things for non-terrestrial networks,” *IEEE Communications Standards Magazine*, vol. 4, no. 4, pp. 49–55, 2020.
- [25] NASA, “Catalog of earth satellite orbits,” *[online]*, 2009, Available:<https://earthobservatory.nasa.gov/features/OrbitsCatalog>.
- [26] A. Guidotti, A. Vanelli-Coralli, M. Caus, J. Bas, G. Colavolpe, T. Foggi, S. Cioni, A. Modenini, and D. Tarchi, “Satellite-enabled lte systems in leo constellations,” in *2017 IEEE International Conference on Communications Workshops (ICC Workshops)*, 2017, pp. 876–881.
- [27] O. Kodheli, S. Andrenacci, N. Maturo, S. Chatzinotas, and F. Zimmer, “Resource allocation approach for differential doppler reduction in nb-iot over leo satellite,” in *2018 9th Advanced Satellite Multimedia Systems Conference and the 15th Signal Processing for Space Communications Workshop (ASMS/SPSC)*, 2018, pp. 1–8.
- [28] 3GPP, “Ts 36.304 technical specification group radio access network; evolved universal terrestrial radio access (e-utra); user equipment (ue) procedures in idle mode (release 14) v14.3.0,” 2017.

- [29] 3GPP, “Tr 25.913, technical specification group radio access network; requirements for evolved ultra (e-utra) and evolved utran (e-utran) (release 9), v9.0.0,” 2009.
- [30] Jaap Beek, Magnus Sandell, and Per Borjesson, “Ml estimation of time and frequency offset in ofdm systems,” *Signal Processing, IEEE Transactions on*, vol. 45, pp. 1800 – 1805, 08 1997.
- [31] H. Bolcskei, “Blind estimation of symbol timing and carrier frequency offset in wireless ofdm systems,” *IEEE Transactions on Communications*, vol. 49, no. 6, pp. 988–999, 2001.
- [32] J. Lin, Z. Hou, Y. Zhou, L. Tian, and J. Shi, “Map estimation based on doppler characterization in broadband and mobile leo satellite communications,” in *2016 IEEE 83rd Vehicular Technology Conference (VTC Spring)*, 2016, pp. 1–5.
- [33] O. Kodheli, S. Andrenacci, N. Maturo, S. Chatzinotas, and F. Zimmer, “Resource allocation approach for differential doppler reduction in nb-iot over leo satellite,” in *2018 9th Advanced Satellite Multimedia Systems Conference and the 15th Signal Processing for Space Communications Workshop (ASMS/SPSC)*, 2018, pp. 1–8.
- [34] 3GPP, “Ts 36.331 radio resource control (rrc) protocol specification (rel. 14),,” 2017.
- [35] Gene H. Golub and Charles F. Van Loan, *Matrix Computations: A comprehensive treatment of numerical linear algebra from the standpoint of both theory and practice*, Johns Hopkins University Press, 2013.
- [36] Monique Petitdidier, Amadou Sy, Axel Garrouste, and Jean Delcourt, “Statistical characteristics of the noise power spectral density in uhf and vhf wind profilers,” *Radio Science*, vol. 32, no. 3, pp. 1229–1247, 1997.

Acknowledgements

I would like to thank my supervisor, Prof. Ing. Alessandro Vanelli Coralli, for his support throughout my graduate project. His great advice has steered my work in the right direction whenever it was needed. It has been a pleasure to work with him on a topic of great interest to me.

I am grateful to my co-supervisors, Dr. Matteo Conti and Dr. Carla Amatetti, for having followed my project, and for providing me valuable comments on my thesis.